Single-Beam Z-Scan: Measurement Techniques and Analysis

Article *in* Journal of Nonlinear Optical Physics & Materials · January 2012

DOI: 10.1142/S0218863597000204

Journal of Nonlinear Optical Physics and Materials
Vol. 6, No. 3 (1997) 251–293

SINGLE-BEAM Z-SCAN: MEASUREMENT TECHNIQUES AND ANALYSIS

P. B. CHAPPLE, J. STAROMLYNSKA, J. A. HERMANN and T. J. MCKAY
Defense Science and Technology Organization,
Electronics and Surveillance Research Laboratory,
PO Box 1500, Salisbury SA 5108, Australia

R. G. MCDUFF
Department of Physics, University of Queensland,
St Lucia, Qld 4072 Australia

Received 8 October 1996

The Z-scan technique is a popular method for measuring degenerate (single frequency) optical nonlinearities using a single laser beam. In order to perform reliable measurements, it is necessary to carefully characterize and control a number of experimental parameters, such as the beam quality, the power and temporal characteristics of the laser, the collection aperture size and position, the sample reflectivity, sample thickness and imperfections in the sample. Failure to control these parameters leads to inaccurate determinations of the nonlinearities. In this paper, we review the theory of Z-scan and examine each of these issues from experimental and theoretical viewpoints. This work will be of interest to anyone who performs Z-scan experiments and to those interested in optical power limiting and nonlinear optical propagation.

1. Introduction

The Z-scan technique[1–2] is an increasingly popular method for the measurement of optical nonlinearities, particularly nonlinear refraction and nonlinear absorption. It has been used to measure nonlinear optical properties of semiconductors,[3–7] dielectrics and glasses,[8–12] organic or carbon-based molecules[13–17] and liquid crystals,[18,19] with nonlinearities ranging from femtosecond[7] to millisecond[20] timescales. It complements and sometimes replaces other measurement techniques such as four-wave mixing. Z-scan has the advantage that it immediately indicates the sign and type of nonlinearity (refractive or absorptive).

In the Z-scan technique, a sample is scanned along the optic axis (the z-direction) through the focus of a single laser beam, while the energy transmitted through an aperture in the far field is recorded as a function of sample position (Fig. 1). It is convenient to plot T, the transmittance normalized to the linear transmittance of the system. A typical Z-scan profile for a thin sample with a

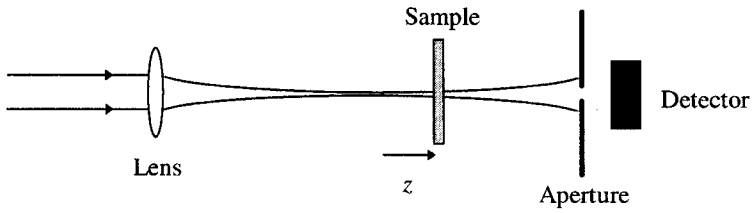

Fig. 1. Experimental arrangement for Z-scan measurement of nonlinear refraction.

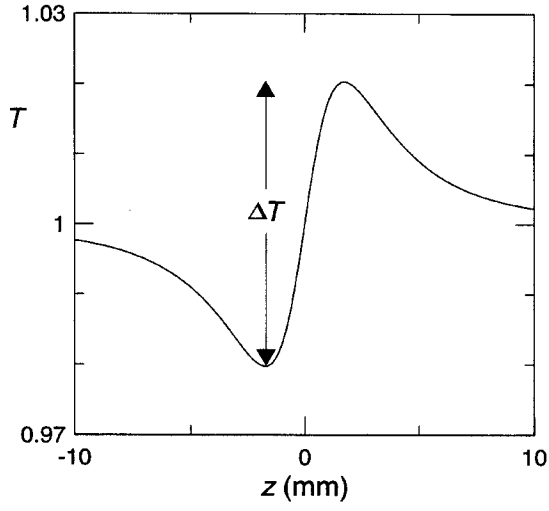

Fig. 2. Z-scan result for a thin self-focusing medium (Eq. (11)). $\Delta\Phi_0 = 0.1$, $z_R = 2$ mm, $z_1 = 10$ m (far field).

purely refractive, positive nonlinearity is shown in Fig. 2. The nonlinearity can often be evaluated from the difference between the maximum and minimum values of the normalized transmittance, ΔT. For a thin optical Kerr medium (where the refractive index varies linearly with irradiance) with nonlinear refractive index coefficient n_I (in units $\mathrm{m^2W^{-1}}$), ΔT is proportional to the nonlinear phase shift $\Delta\Phi_0$ on the axis with the sample at the waist,[2] and hence to n_I:

$$\Delta T = 0.406|\Delta\Phi_0|\,, \tag{1}$$

where $\Delta\Phi_0 = kn_I I_0 L_{\mathrm{eff}}$. Here $k = 2\pi/\lambda$, λ is the wavelength, I_0 is the axial irradiance at the waist and L_{eff} is the effective sample length. This is given by $L_{\mathrm{eff}} = (1 - e^{-\alpha_0 L})/\alpha_0$, where L is the true sample length and α_0 is the linear absorption coefficient ($L_{\mathrm{eff}} = L$ in the absence of linear absorption). Equation (1) is correct to first order in I_0 (the weak interaction regime), for a Gaussian profile laser beam and an infinitesimal aperture or pinhole at the far field.

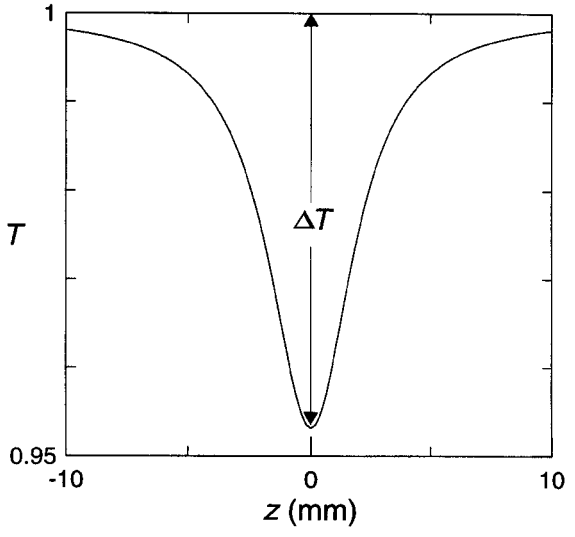

Fig. 3. Z-scan result for a thin absorber (Eq. (21)). $Q_0 = 0.1$; $z_R = 2$ mm.

For Z-scan measurements of nonlinear absorption, the aperture in Fig. 1 is usually removed so that the total beam power or energy can be collected. A Z-scan profile for a thin nonlinear absorber is depicted in Fig. 3. For an absorption coefficient which varies linearly with irradiance, the coefficient of nonlinear absorption α_I (in units mW^{-1}) can be evaluated using[2]

$$\Delta T = \left| 1 - \frac{1}{Q_0} \ln(1 + Q_0) \right| , \tag{2}$$

with $Q_0 = \alpha_I I_0 L_{\mathrm{eff}}$. Note that Eq. (2) is correct to all orders of I_0.

The Z-scan method is attractive owing to its experimental simplicity (it is a single beam technique), the fact that it yields both the sign and the magnitude of the nonlinearity and the fact that n_I and α_I may be easily extracted with a minimal amount of analysis. A further advantage is the close similarity between the Z-scan and optical power limiter geometries. Detailed Z-scan studies not only give important information on the nonlinear optical characteristics of a material but also yield vital information regarding optimization of the optical power limiting geometry such as the optimum sample position and optimum sample thickness. This makes Z-scan the preferred technique when assessing materials for an optical power limiting application.

Despite the apparent experimental simplicity of the Z-scan technique, great care has to be taken with the experimental measurements to ensure reliable results. There are several factors which may lead to poor Z-scan profiles and unreliable data if their effects are not understood. They include: (i) a poor input beam spatial profile, (ii) poor understanding of the temporal characteristics of the laser (iii) fluctuating laser power, (iv) etalon effects in non-ar-coated samples, (v) sample

thickness exceeding the "thin sample" regime (vi) inappropriate size or distance, or poor alignment of the aperture for measuring on-axis transmittance, (vii) wedge and lens effects and other defects in the sample, and (viii) laser power exceeding the range of the low power regime, in which the nonlinear effects can be calculated from expressions correct to first order in irradiance. To measure optical nonlinearities absolutely and accurately, all of the above experimental parameters must be carefully controlled, and proper corrections need to be made in the experimental analysis.

As pointed out by Bridges *et al.*,[21] the requirements for controlling all these parameters can be relaxed somewhat when the nonlinearity of a test sample is measured relative to that of a reference sample. This is an excellent approach, provided that one has a suitable reference sample. Often one does not have a sample with a well characterized nonlinearity for the particular wavelength and pulse length regime of interest. This is particularly so when nonlinear absorption and refraction are both involved. In this case, the reference sample would need to have the same ratio of absorptive and refractive nonlinearities.

Part 2 of the present paper sets up a theoretical framework needed for discussing Z-scan measurements, introducing previously published equations of importance and also presenting significant new material. The Z-scan technique for a thin nonlinear refractor is discussed, and the discussion is then broadened to allow for nonlinear absorption. Equations are introduced to describe the irradiance away from the optical axis, as needed for discussing finite aperture effects and aperture misalignment. An improvement to the conventional approach is suggested for separating the nonlinear refraction result when absorptive and refractive effects are simultaneously present. Next, the on-axis description for thin media is extended to deal with thick media. This theory is not only important for understanding the sample thickness requirements in Z-scan experiments, but is also very useful for modeling optical power limiters. Finally, numerical calculations using the Gaussian-Laguerre decomposition method are discussed. These allow the study of nonlinear effects to be extended to higher power levels, where the analytic calculations correct to the first order in irradiance are no longer valid. These numerical results indicate the regime of validity of first-order analytical theory, and give some guidance in correcting the first-order calculations to take account of higher-order effects.

In Part 3 the experimental sources of inaccuracy listed above are analyzed and methods are suggested for overcoming some of the problems. The impact of a poor spatial input beam profile is examined and it is established that for a standard deviational error in ΔT of less than 5%, the spatial profile of the laser beam should have an M^2 value of less than 1.1 for nonlinear refraction, or 1.3 for nonlinear absorption, and that corrections should be made for a non-unity value of M^2. Suggestions are given on how to achieve a good beam profile.

The importance of the laser's temporal profile is discussed, in the context of pulsed laser experiments. This profile should be recorded and analyzed, for accurate measurements of nonlinearities. The effect of laser power fluctuations upon the

apertureless Z-scan profiles is illustrated, and a technique for recovering the data is outlined.

The effects of unwanted surface reflections are described, and it is emphasized that the samples should be anti-reflection-coated, at least on their rear surfaces. Sample thickness is then discussed, and it is shown that for a nonlinear refractor ΔT is more than 6% below the thin sample value if the sample thickness is greater than $n_0 z_R$, the Rayleigh length of the beam waist within the medium. For nonlinear absorption, the reduction in ΔT under these conditions is 7%.

Results are also presented highlighting the effect of aperture size upon the ΔT value for nonlinear refraction measurements, and guidelines are given for choosing an appropriate aperture size. The impact of the distance to the aperture is also considered. As the Z-scan technique is a far field measurement method in practice it is important that the term "far-field" be defined. At a distance of 10 Rayleigh lengths between the beam waist and the aperture, there is an 18% change in the T values, compared with the values at the far-field. However, the error in ΔT is only 1% because both the peak and trough move in the same direction. Modeling studies of the effect of poor aperture alignment on the Z-scan profile are presented. It is shown that if the sample is wedged, best results are obtained if alignment of the aperture is carried out with the sample positioned at the center of the scan. Modeling studies also establish the effects which occur if the sample has a lens-like profile or if it exhibits surface roughness or scratches. We find that the technique of subtracting low power Z-scans from high power ones, as recommended by Sheik-Bahae *et al.*,[2] works well for extracting the nonlinear result when there are surface imperfections. Finally, we briefly discuss extensions of Z-scan such as the EZ-scan technique.[22–24]

This paper will be useful as a reference document for those wishing to use the Z-scan technique. It should also prove to be of value to those involved in the study and design of optical power limiters. While the theory is based on third-order optical nonlinearities (see Eqs. (5) and (15)), the principles and experimental techniques discussed are also applicable when higher-order or other nonlinearities are present. Experimentalists primarily interested in Z-scan may choose to omit Part 2, which is mathematical in nature, and to proceed to the discussion of experimental parameters in Part 3. It should be noted, however, that this discussion draws heavily on the theoretical results of Part 2.

2. Background Theory and Equations

2.1. *Thin Nonlinear Refractor*

It is helpful at this point to introduce some of the theory and equations needed to discuss Z-scans with a thin nonlinear sample. The sample at position z has a linear refractive index n_0 and a more general refractive index n, which can depend on the irradiance $I(x, y, z)$, or $I(r, z)$ for radial symmetry. For a Kerr nonlinearity,

$$n = n_0 + n_I I = n_0 + \frac{1}{2} n_2 |E|^2 , \tag{3}$$

where E is the (complex) electric field amplitude within the sample. The nonlinear refractive coefficient n_I is identical to γ used by Weber *et al.*,[25] Sheik-Bahae *et al.*[2] and others, and has also been variously labeled n_2 and n_s. We use the symbol n_I in order to highlight its association with n_0 and n_2, with the subscript symbolizing irradiance or intensity. Equation (3) is consistent in form with Eq. (13) describing the irradiance-dependent absorption coefficient. The coefficients n_I and n_2 are related by

$$n_I(\mathrm{m^2W^{-1}}) = \frac{40\pi n_2(\mathrm{esu})}{n_0 c(\mathrm{ms^{-1}})}\,, \tag{4}$$

where c is the speed of light in a vacuum. The nonlinear refractive coefficient is proportional to the real part of the third-order nonlinear susceptibility $\chi^{(3)}$:

$$n_I(\mathrm{m^2W^{-1}}) = \frac{120\pi^2}{{n_0}^2 c(\mathrm{ms^{-1}})}\mathrm{Re}\chi^{(3)}(\omega,\omega,-\omega)(\mathrm{esu})\,, \tag{5}$$

where ω is the angular frequency of the field. Unfortunately there are various numerical conventions for nonlinear susceptibilities in use. Different conventions and systems of units are discussed in the Appendix.

In a thin nonlinear refractor, there is insufficient path length for the beam to change its size or shape as it propagates through the medium. The effect of the nonlinearity is a phase change $\Delta\phi$ at the nonlinear medium, given in the paraxial approximation by

$$\Delta\phi(r,z) = \int_z^{z+L} kn_I I(r,z')dz' = kn_I I(r,z)L_{\mathrm{eff}}\,. \tag{6}$$

Here, the irradiance of a Gaussian beam, with waist size w_0 and waist at $z = 0$, is

$$I(r,z) = \frac{I_0 e^{-2r^2/w(z)^2}}{1 + z^2/{z_R}^2}\,, \tag{7}$$

where

$$w(z)^2 = {w_0}^2(1 + z^2/{z_R}^2) \tag{8}$$

and the Rayleigh length is $z_R = \pi {w_0}^2/\lambda$.

The irradiance at the position z_1 of the observation plane, which is beyond the nonlinear sample, can be calculated by incorporating the phase shift at the sample and using diffraction theory.[26] It is useful to define a linear phase parameter

$$v = -\frac{1}{z_R}\left(z + \frac{{z_R}^2 + z^2}{z_1 - z}\right)\,. \tag{9}$$

When z_1 is much larger than z and z_R, $v \approx -z/z_R$. (More generally, v is the cotangent of the on-axis phase change of the low power beam, relative to a plane wave, as the beam propagates from the cell position z to the observation plane.) It is also useful to define the nonlinear phase shift parameter[2]

$$\Delta\phi_0 \equiv kn_I I(0,z)L_{\mathrm{eff}} = \frac{\Delta\Phi_0}{1 + z^2/{z_R}^2}\,, \tag{10}$$

where $\Delta\Phi_0 = kn_I I_0 L_{\text{eff}}$ (as in Eq. (1)). In the absence of nonlinear absorption, $\Delta\phi_0$ is the same as the on-axis phase shift $\Delta\phi(0,z)$. The parameters $\Delta\Phi_0$ and $\Delta\phi_0$ are equivalent to κ' and $\hat{K}'$ defined by Hermann.[27,28] The normalized transmittance T measured using an infinitesimal aperture at the observation plane is given to first order in irradiance by[27]

$$T = 1 - \frac{4\Delta\phi_0 v}{9+v^2}\,, \tag{11}$$

as plotted in Fig. 2. For a self-focusing medium ($\Delta\phi_0 > 0$) there is a minimum transmittance when the medium lies before the waist ($z < 0$), because the medium focuses the beam to a smaller waist, increasing the beam divergence beyond it. There is correspondingly a maximum when the medium lies after the waist, as the focusing reduces the beam divergence. The opposite behavior occurs for a defocusing medium ($\Delta\phi_0 < 0$). Differentiation of Eq. (11) with $z_1 \to \infty$ gives rise to Eq. (1) for ΔT, and the distance between the z-positions of the minimum and maximum under these conditions is $\Delta z = 1.717 z_R$.

Effects of second and third order in irradiance become important as the laser power is increased. For example, when the sample is located at the waist and the pinhole is at the far-field ($v = 0$), the lowest-order effect on T is of the second order. In this case, an axial shift in the waist position is associated with a reduction in the effective waist size and a reduction in T proportional to the square of the irradiance. To the third order, the result for T is[27]

$$T = 1 - \frac{4\Delta\phi_0 v}{9+v^2} - \frac{4\Delta{\phi_0}^2(5-3v^2)}{(9+v^2)(25+v^2)} + \frac{32\Delta{\phi_0}^3 v(11-v^2)}{(9+v^2)(25+v^2)(49+v^2)}\,. \tag{12}$$

2.2. *Nonlinear Absorber/Refractor*

Nonlinear absorptive effects such as two-photon absorption can be incorporated using an irradiance-dependent absorption coefficient α:

$$\alpha = \alpha_0 + \alpha_I I = \alpha_0 + \alpha_2 |E|^2\,, \tag{13}$$

Here α_I is the same as the parameter β as used by Weber *et al.*,[25] Sheik-Bahae *et al.*[2] and others. Equation (13) is consistent in form with Eq. (3) describing the irradiance-dependent refraction coefficient. We use the symbol α_I to highlight its association with α_0 and α_2, in correspondence with the choice of symbols for nonlinear refraction. The nonlinear absorption coefficients α_I and α_2 are related by

$$\alpha_I(\text{mW}^{-1}) = \frac{8000\pi\alpha_2(\text{esu})}{c(\text{ms}^{-1})n_0}\,. \tag{14}$$

This is the absorptive counterpart to the expression given in Eq. (4) relating the nonlinear refractive coefficients. By analogy to Eq. (5), the nonlinear absorptive coefficient is proportional to the imaginary part of the third-order nonlinear susceptibility $\chi^{(3)}$:

$$\alpha_I(\text{mW}^{-1}) = \frac{240\pi^2\omega}{{n_0}^2 c^2(\text{ms}^{-1})}\text{Im}\chi^{(3)}(\omega,\omega,-\omega)(\text{esu})\,, \tag{15}$$

where ω is the angular frequency of the field. Different numerical conventions and systems of units for nonlinear susceptibilities are discussed in the Appendix.

The effect of the nonlinear absorption is to reduce the irradiance at the exit face of the sample to an amount $I_e(r,z)$, given in the paraxial approximation by[2]

$$I_e(r,z) = I(r,z) - \int_z^{z+L} [\alpha_0 + \alpha_I I(r,z')]I(r,z')dz' = \frac{I(r,z)e^{-\alpha_0 L}}{1+\alpha_I I(r,z)L_{\text{eff}}}. \quad (16)$$

The nonlinear phase shift associated with n_I is reduced by the nonlinear absorption of the beam:

$$\Delta\phi(r,z) = \int_z^{z+L} kn_I I(r,z')dz' = \frac{kn_I}{\alpha_I}\ln(1+\alpha_I I(r,z)L_{\text{eff}}). \quad (17)$$

The nonlinear transmittance can be determined for simultaneous nonlinear refraction and nonlinear absorption, monitored using an infinitesimal aperture. It is useful to define the on-axis absorptive parameter[2]

$$q_0 \equiv \alpha_I I(0,z)L_{\text{eff}} = \frac{Q_0}{1+z^2/{z_R}^2}, \quad (18)$$

where we define $Q_0 = \alpha_I I_0 L_{\text{eff}}$ (as in Eq. (2)). This equation is the absorptive counterpart of Eq. (10). When $q_0 \ll 1$, this quantity represents the proportion of light absorbed on-axis by the nonlinear process. The parameters Q_0 and q_0 are double, but otherwise equivalent to, the parameters κ'' and $\hat{K}''$ defined by Hermann.[27,28] The analytic result for T, correct to the second order in irradiance is[27]

$$T = 1 - \frac{4\Delta\phi_0 v + q_0(3+v^2)}{9+v^2} - \frac{4{\Delta\phi_0}^2(5-3v^2) - 8\Delta\phi_0 q_0 v(9+v^2) - {q_0}^2(40+17v^2+v^4)}{(9+v^2)(25+v^2)} \quad (19)$$

Some caution must be exercised in applying this low irradiance result, since the convergence properties of the terms for nonlinear absorption are not as good as those for nonlinear refraction with thin media. This is the case because the nonlinear absorption of light near the entrance face of the medium reduces the subsequent nonlinear absorption (and nonlinear refraction), making higher-order effects more significant. The impact of higher-order effects upon measurements of nonlinearities will be discussed in Sec. 2.5. The expression for T correct to all orders of irradiance is[28]

$$T = \left|{}_2F_1\left(\frac{1}{2} - i\Delta\phi_0/q_0, \frac{1}{2}(1+iv); \frac{1}{2}(3+iv); -q_0\right)\right|^2, \quad (20)$$

where ${}_2F_1$ is a hypergeometric function.[29]

As mentioned in Part 1, nonlinear absorption can be measured by removing the far-field aperture and measuring the total power transmitted by the nonlinear

medium. In this situation, nonlinear refraction in the thin medium has no influence upon the signal. The result for T, correct to all orders of irradiance, is[2]

$$T = \frac{1}{q_0} \ln(1 + q_0), \tag{21}$$

as plotted in Fig. 3. This yields immediately the result for ΔT given in Eq. (2).

A straightforward method for determining n_I and α_I for a simultaneously nonlinear refracting and absorbing sample has been discussed by Sheik-Bahae *et al.*[2] It involves dividing the normalized transmittance obtained using a pinhole or aperture, $T_a(z)$, by the normalized transmittance obtained *without* an aperture, $T_{na}(z)$. The resulting function is devoid of most of the nonlinear absorptive features, leaving principally the refractive contribution. The resulting ΔT value agrees with the value for a purely refractive nonlinearity to within 10%, provided that $Q_0 \leq 1$ and $\alpha_I/(2kn_I) \leq 1$.[2]

A higher accuracy may be achieved dividing instead by $T_{na}(z/1.25)^{0.67}$, since the first-order term in q_0 in this expression has a similar z-dependence to the first-order term in q_0 in Eq. (19). The resulting nonlinear transmittance $T_{\text{refr}}(z)$ now closely matches that obtained for a purely refractive nonlinearity. The extension of this correction to allow for finite aperture sizes is considered in the next section.

Time-dependence of the irradiance has not been explicitly included in the above equations. This issue will be discussed in Sec. 3.2.

2.3. *Off-Axis Irradiance*

The equations in Sec. 2.2 describe the nonlinear transmittance as would be measured using an infinitesimal pinhole aperture centered on the optic axis. For analyzing finite aperture effects and the effects of aperture misalignment, it is useful to calculate a more general irradiance $I(r, z_1)$ at radial position r and axial position z_1 (at the observation plane, beyond the nonlinear medium). To all orders of irradiance, this is given by

$$I(r, z_1) = \frac{k^2 {w_0}^2 I_0 e^{-\alpha_0 L}}{w(z)^2 (z_1 - z)^2} \left| \int_0^\infty J_0\left(\frac{krr'}{z_1 - z}\right) \exp\left(\frac{-r'^2(1 + iv)}{w(z)^2}\right) \right.$$
$$\left. \times \left[1 + q_0 \exp\left(\frac{-2r'^2}{w(z)^2}\right)\right]^{-\frac{1}{2} + i\Delta\phi_0/q_0} r' dr' \right|^2, \tag{22}$$

where J_0 is a Bessel function and the beam size $w(z)$ is given by Eq. (8). This expression may be evaluated to first-order in irradiance, and yields the new result

$$\frac{I(r, z_1)}{I_{\text{lin}}(0, z_1)} = \exp(-2\rho^2) + \frac{1}{9 + v^2} \exp\left(-4\rho^2 \frac{3 + v^2}{9 + v^2}\right) \times \{2\Delta\phi_0[(3 + v^2)\sin\Psi$$
$$- 2v\cos\Psi] - q_0[(3 + v^2)\cos\Psi - 2v\sin\Psi]\}, \tag{23}$$

where the linear on-axis irradiance is

$$I_{\text{lin}}(0, z_1) = \frac{I_0 e^{-\alpha_0 L}}{1 + {z_1}^2/{z_R}^2}, \tag{24}$$

$\rho = r/w(z_1)$ and $\Psi = 8\rho^2 v/(9 + v^2)$. (Note that the special refractive case of Eq. (23) [$q_0 = 0$] has been given in Ref. 30). Equation (23) is useful for analyzing Z-scan results with a misaligned aperture or an imperfect sample (Sec. 3.8 and 3.9).

One may integrate $I(r, z_1)$ into Eq. (22) or (23) to obtain the Z-scan result for a finite aperture of radius r_a. It is useful to define the linear transmittance S of the aperture for a Gaussian input beam:[2]

$$S = 1 - \exp(-2r_a^2/w(z_1)^2). \tag{25}$$

The pinhole aperture limit is $S = 0$, while the open aperture (no aperture) case corresponds to $S = 1$. The first-order expression for the nonlinear transmittance is[28]

$$T = P_t/[P_i \exp(-\alpha_0 L)S] = 1 - \frac{q_0}{2S} + \frac{(1-S)^\mu}{S} \cdot \left(\Delta\phi_0 \sin\varphi + \frac{1}{2} q_0 \cos\varphi\right), \tag{26}$$

where P_i and P_t are the incident and transmitted powers, $\mu = 2(3 + v^2)/(9 + v^2)$ and $\varphi = [\ln(1 - S)] \cdot 4v/(9 + v^2)$. Finite aperture effects are discussed further in Sec. 3.6.

As discussed in Sec. 2.2, the refractive contribution to the nonlinearity may be isolated from the absorptive contribution by dividing the normalized transmittance through a pinhole or aperture, $T_a(z)$, by the normalized transmittance with no aperture, $T_{na}(z)$. A more accurate approach is to evaluate the refractive part of $T(z)$ as

$$T_{\text{refr}}(z) = \frac{T_a(z)}{[T_{na}(z/1.25)]^p}, \tag{27}$$

where $p = S + 0.67(1 - S)^2$. This equation is plotted in Fig. 4, together with the theoretical value of $T_{\text{refr}}(z)$ calculated from Eq. (26) (with $q_0 = 0$). Equation (27) provides an improved method of evaluating the refractive contribution to $T_a(z)$, and gives a more accurate value for the refractive contribution to ΔT.

2.4. *Thick Nonlinear Sample*

One possible method of analyzing Z-scan data with thick samples is to use the aberrationless (or constant shape) approximation.[31–33] In this approximation the assumption is made that the radial variation of the sample's refractive index is quadratic and hence, the beam propagating through the nonlinear medium retains a Gaussian spatial profile. Applying this approximation requires the introduction of an empirical factor (sometimes denoted a) which purports to correct for the fact that the refractive index variation is not truly quadratic. Use of the aberrationless approach to analyze Z-scan data may produce significant inaccuracies when there are large nonlinear phase shifts and also when analyzing thick sample

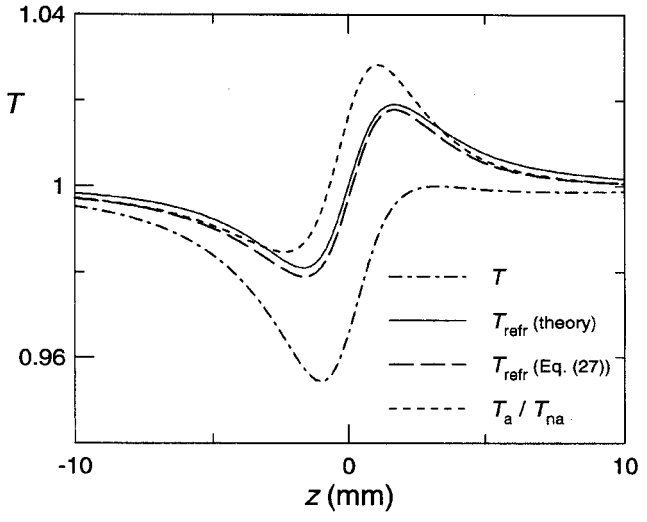

Fig. 4. Extraction of the refractive contribution to the nonlinearity. $\Delta|\Phi_0 = Q_0 = 0.1$, $z_R = 2$ mm, $S = 0.2$.

data.[32] Often it is difficult to determine the most appropriate value of a. In short, the approximation of a quadratic refractive index profile is not always a good approximation.

Another approach which we investigated for modeling nonlinear propagation through thick media is that of Paré and Bélanger.[34] These authors made use of the fact that, for a Kerr-type nonlinear refractor, the second moments of position ${w_x}^2/4$ and ${w_y}^2/4$ (measures of the beam width) follow a simple quadratic dependence on the axial position z. While this is a valid approach, knowledge of w_x and w_y does not provide sufficient information to allow the irradiance distribution to be calculated, and the latter is needed for determining the transmittance of the Z-scan aperture and the propagation of the field beyond the nonlinear medium. Our preferred approach for modeling Z-scans is to use the first-order theory of Hermann and McDuff[35] for weak nonlinearities, and a numerical approach (Sec. 2.5) for the case of higher irradiances, where there is strong nonlinear refraction or absorption.

A thick nonlinear sample of length L is shown in Fig. 5. The linear refractive index n_0 reduces the rate at which the beam evolves with distance in the medium, which causes an axial shift $L(1-1/n_0)$ in the beam beyond the sample. The distance from the unshifted waist to the entrance face is z_a; the distance from the shifted waist to the exit face is $z_b = z_a + L/n_0$; ${z_1}'$ is the distance from the shifted waist to the observation plane. It is useful to define parameters v_a and v_b, as in Eq. (9), corresponding to the entrance and exit faces of the cell:

$$v_i = -\frac{1}{z_R}\left(z_i + \frac{{z_R}^2 + {z_i}^2}{{z_1}' - z_i}\right) \quad \text{for } i = a, b\,. \tag{28}$$

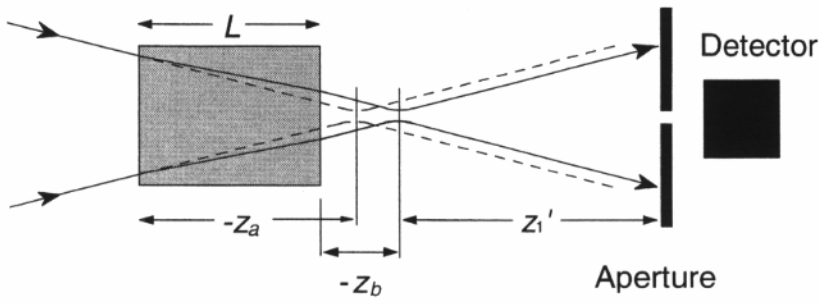

Fig. 5. The thick medium scenario.

When the sample is much longer than one Rayleigh length, the length of the interaction region is determined by the Rayleigh length $n_0 z_R$ of the waist within the medium, rather than the sample length. Therefore for thick sample equations we replace the nonlinear phase-shift and absorption parameters $\Delta\Phi_0$ and Q_0 of Eqs. (1) and (2) with $\Delta\Phi_{0R} = kn_I I_0 n_0 z_R$ and $Q_{0R} = \alpha_I I_0 n_0 z_R$. These parameters correspond to the parameters $\beta(= 2\Delta\Phi_{0R})$ and $\alpha(= Q_{0R})$ used by Hermann and McDuff[35] (see the Appendix).

Hermann and McDuff[35] have derived an analytic expression for the nonlinear transmittance T of a thick sample, correct to first order in irradiance, for a pinhole aperture in the far field, in the absence of linear absorption. In a slightly different form, the expression may be written:

$$T = 1 - \frac{1}{4}\left\{\Delta\Phi_{0R}\ln\left(\frac{1+{v_a}^2}{9+{v_a}^2}\cdot\frac{9+{v_b}^2}{1+{v_b}^2}\right)\right.$$
$$\left. + Q_{0R}\left[\tan^{-1}(v_a) + \tan^{-1}(v_a/3) - \tan^{-1}(v_b) - \tan^{-1}(v_b/3)\right]\right\}. \quad (29)$$

In the limit that $L \ll z_R$, this equation is consistent with the thin sample equation (19). Equation (29) is plotted in Fig. 6 (solid curve), for both refractive and absorptive nonlinearities. It is clear that the thin medium features shown in Figs. 2 and 3 are now extended over a range of z-values corresponding to the length of the sample. In the case of pure self-focusing, a peak in the transmittance occurs when the front (entrance) surface of the sample is located at the beam waist, because self-focusing reduces the beam divergence within the medium beyond the waist. A minimum occurs when the rear (exit) surface is located at the (shifted) waist, because self-focusing reduces the waist size, thereby increasing the beam divergence outside the medium beyond the waist. When the waist region lies within the sample, these effects tend to nullify one another. In the case of nonlinear absorption, the absorption is close its maximum value whenever the waist region lies essentially within the medium. Chapple *et al.*[36] have experimentally verified the accuracy of Eq. (29) for (self-focusing) samples of CS_2.

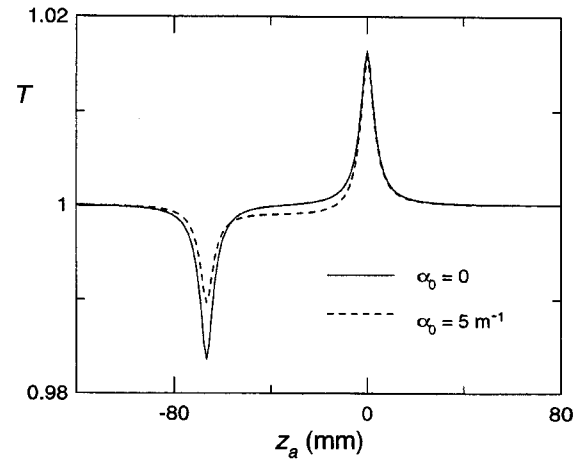

(a)

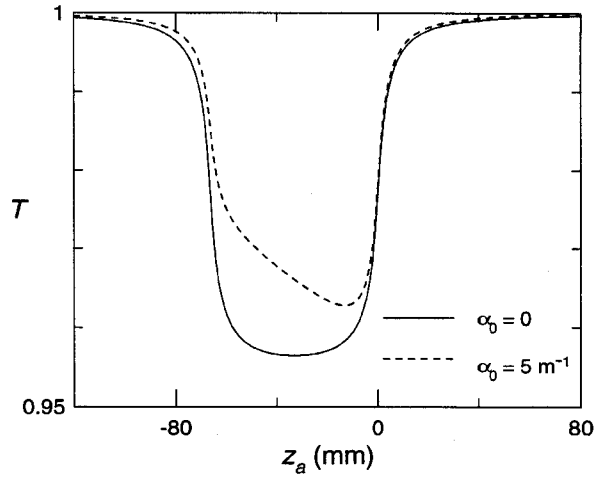

(b)

Fig. 6. Z-scan results for a thick medium, calculated from Eq. (29) ($\alpha_0 = 0$) and Eq. (36) ($\alpha_0 \neq 0$). $L = 0.1$ m, $n_0 = 1.5$, $z_R = 2$ mm. (a) Nonlinear refraction: $\Delta\Phi_{0R} = 0.03$. (b) Nonlinear absorption: $Q_{0R} = 0.03$.

The ΔT value can be calculated by differentiating Eq. (29). For a purely refractive nonlinearity, the far-field result is[35]

$$\Delta T = \frac{|\Delta\Phi_{0R}|}{2} \ln\left[\frac{9+\Omega-\Gamma}{1+\Omega-\Gamma} \cdot \frac{1+\Omega+\Gamma}{9+\Omega+\Gamma}\right], \tag{30}$$

where

$$\Omega = \eta + \frac{1}{3}{\zeta_m}^2 ,$$

$$\Gamma = \zeta_m \left(\eta + \frac{1}{12}{\zeta_m}^2\right)^{1/2} ,$$

$$\eta = -\frac{5}{3} + \left[3 + \frac{1}{9}\left(5 + \frac{1}{2}{\zeta_m}^2\right)^2\right]^{1/2}$$

and

$$\zeta_m = L/(n_0 z_R) .$$

Some implications of this analysis are discussed in Sec. 3.5. As $\zeta_m \to \infty$ (thick sample limit), ΔT approaches $|\Delta\Phi_{0R}| \ln 3$.

For a purely absorptive nonlinearity, the far-field on-axis transmittance is symmetrical as z_a is varied about $z_a = -L/(2n_0)$. By evaluating Eq. (29) at this position, we obtain the new result

$$\Delta T = \frac{1}{2}|Q_{0R}| \cdot \left[\tan^{-1}\left(\frac{1}{2}\zeta_m\right) + \tan^{-1}\left(\frac{1}{6}\zeta_m\right)\right] . \tag{31}$$

The first-order thick sample result for T can be related simply to the first-order result $T_{\text{thin}}(z)$ for a thin sample of length δL. We write this as

$$T_{\text{thin}}(z) = 1 + \tau(z)\delta L ,$$

where, for an on-axis pinhole at the observation plane, we obtain from Eq. (19):

$$\tau(z) = -\frac{4\Delta\Phi_{0R} v(z) + Q_{0R}(3 + v(z)^2)}{n_0 z_R (1 + z^2/{z_R}^2)(9 + v(z)^2)} , \tag{32}$$

with $v(z)$ given in Eq. (9). To establish the correspondence, note that moving the thick sample by a positive increment dz_a, while holding thickness L constant, is formally equivalent to removing from the sample a slice of thickness dz_a at the front face (at z_a) and replacing it at the rear face (at distance z_b from the shifted waist). Because we are considering a first-order result, we can simply add the contributions to T from the different slices; thus we should subtract $\tau(z_a)dz_a$ and add $\tau(z_b)dz_a$. There is an additional effect that removing the slice at z_a causes a linear axial shift in the beam of $-dz_a(1 - 1/n_0)$ between z_a and z_b. The effect on T is equivalent to that of moving all the intermediate slices of the sample by an amount $dz_a(1 - 1/n_0)$. Thus

$$dT = \left[-\tau(z_a) + \tau(z_b) + \frac{dT}{dz_a}(1 - 1/n_0)\right] dz_a$$

or

$$\frac{dT}{dz_a} = n_0[\tau(z_b) - \tau(z_a)]; \quad z_b = z_a + L/n_0 . \tag{33}$$

Equation (29) is an exact solution of this differential equation, as can be verified using the identity

$$\frac{dv_i}{dz_i} = -\frac{1}{z_R} \cdot \frac{1 + {v_i}^2}{1 + {z_i}^2/{z_R}^2} \quad \text{for } i = a, b\,.$$

This line of argument can be extended to take linear absorption into account. The resulting differential equation (in the paraxial approximation) is now found to be

$$\frac{dT}{dz_a} = n_0[\alpha_0(T-1) + \tau(z_b)e^{-\alpha_0 L} - \tau(z_a)]; \quad z_b = z_a + L/n_0\,. \tag{34}$$

The appropriate solution of this equation for the first-order nonlinear transmittance is

$$T = 1 + \int_0^L \tau(z_a + z/n_0)e^{-\alpha_0 z'}\,dz'\,. \tag{35}$$

The precise form of this integral is generally complicated, and may be evaluated in terms of the exponential integral functions.[29] In the far-field, however ($v(z) \approx -z/z_R$), taking $\alpha_0 n_0 z_R \ll 1$ and $\alpha_0 n_0 z_i$ less than or of the order of 1 (for $i = a, b$), we can approximate the exponential $\exp(-\alpha_0 z')$ by a linear function of $v(z')$, to obtain:

$$T = 1 + \frac{1}{4}e^{\alpha_0 n_0 z_a}\left[\left(\Delta\Phi_{0R} + \frac{1}{2}Q_{0R}A\right)\ln(1+v^2) - \left(\Delta\Phi_{0R} - \frac{3}{2}Q_{0R}A\right)\ln(9+v^2)\right.$$
$$\left. + (Q_{0R} - 2\Delta\Phi_{0R}A)\tan^{-1}v + (Q_{0R} + 6\Delta\Phi_{0R}A)\tan^{-1}(v/3)\right]_{v_a}^{v_b} \tag{36}$$

where $A = \alpha_0 n_0 z_R$.

Results calculated using this equation are plotted, together with the corresponding results in the absence of linear absorption, in Fig. 6. Clearly, linear absorption reduces the nonlinear effects associated with the rear (beam exit) end of the cell more significantly than those of the front (beam entrance) end, both for refractive and absorptive nonlinearities.

The arguments given above can be generalized to describe the off-axis irradiance, and first-order transmittances can be determined for the finite aperture and open aperture situations. For the thick medium Z-scan without an aperture, the relevant thin-medium result is given by the first-order contribution in Eq. (21):

$$\tau(z) = -\frac{Q_{0R}}{2n_0 z_R(1 + z^2/{z_R}^2)}\,, \tag{37}$$

which can be inserted in Eq. (35). With $\alpha_0 n_0 z_R \ll 1$ and $\alpha_0 n_0 z_i$ less than or of the order of 1 (for $i = a, b$), we obtain

$$T = 1 - \frac{1}{2}Q_{0R}e^{\alpha_0 n_0 z_a}\left[\tan^{-1}(z/z_R) - \frac{1}{2}A\ln(1 + z^2/{z_R}^2)\right]_{z_a}^{z_b}\,. \tag{38}$$

For the thick medium Z-scan without an aperture, and in the absence of linear absorption, we obtain the simple result

$$T = 1 - \frac{1}{2}Q_{0R}\left[\tan^{-1}(z_b/z_R) - \tan^{-1}(z_a/z_R)\right] \tag{39}$$

(analogous to Eq. (29) for the pinhole aperture). Evaluating Eq. (39) at the midpoint $z_a = -L/(2n_0)$, we obtain

$$\Delta T = |Q_{0R}| \cdot \tan^{-1}\left(\frac{1}{2}\zeta_m\right). \tag{40}$$

On comparing this equation with Eq. (31), we see that, in the thick sample limit and at the far field, $\Delta T = \frac{1}{2}\pi|Q_{0R}|$, both for $S = 0$ and $S = 1$, and in fact it can be shown that there is no dependence upon S. This indicates that, for a thick nonlinear absorber ($L \gg z_R$) and a Gaussian beam and with the absorption indicated by Eq. (13), the outgoing beam profile is a uniformly scaled version of the linear beam profile, ie. the thick absorber absorbs uniformly across the profile of the Gaussian beam. Modeling described in the next section indicates that this first-order result is also a useful approximation when higher-order effects become important.

2.5. *Numerical Solutions*

The equations of the previous section are valid only to first order in irradiance, and are therefore generally applicable only when $T \approx 1$. Higher-order effects are often important in laboratory situations.[36] They can be calculated using numerical techniques, and this also allows for convenient inclusion of other optical nonlinearities. Three such techniques are the Gaussian beam expansion used by Sheik-Bahae *et al.*,[2,37] the Gaussian-Laguerre modal decomposition approach of McDuff *et al.*[38,39] and the fast Fourier transform technique of Hughes *et al.*[40]

While the Gaussian beam expansion technique works well for small perturbations of the field away from a Gaussian shape, it suffers from severe convergence problems for larger perturbations. The Gaussian-Laguerre technique, which expresses the electric field in terms of an orthogonal basis set of propagation modes, is more generally applicable. The fast Fourier transform technique is also appropriate, although there can be difficulties in choosing an appropriate computation grid size to accommodate changes in the beam's spatial dimensions as it propagates between the waist and the far field.

We have modeled propagation through a thick nonlinear medium using the Gaussian-Laguerre technique, by dividing the medium into slices much thinner than one Rayleigh length. The nonlinear refraction or absorption induced by each slice is applied to the electric field incident on the slice, and linear propagation is assumed between slices. Figure 7 shows results calculated in this way for strong nonlinear refraction and absorption. The agreement with the lowest-order theory (Fig. 6) is good for weak nonlinearities ($\Delta T \ll 1$).

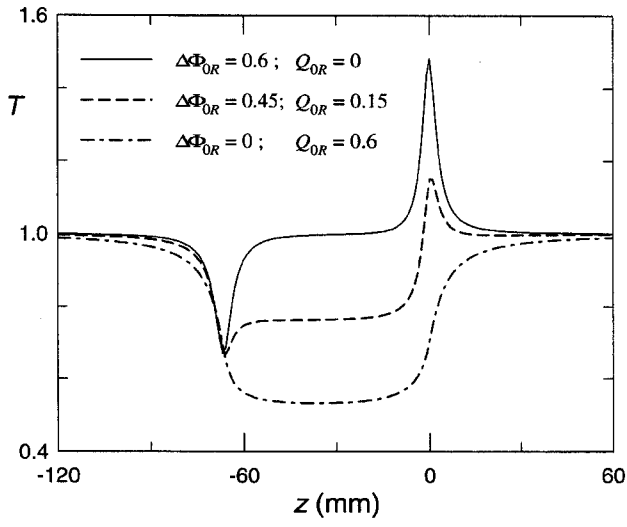

Fig. 7. Numerically calculated Z-scan results for a thick medium. Here $L = 0.1$ m, $n_0 = 1.5$, $\alpha_0 = 0$, $z_R = 2$ mm and $S = 0.01$.

Figure 8 shows the calculated dependence of the normalized transmittance T on the irradiance-dependent or nonlinear interaction parameters Φ_0, Φ_{0R}, Q_0 and Q_{0R}, for thin and thick media. These results reveal the regime of reliability of the analytical theory. For the thin nonlinear refractor (Fig. 8(a)), the maximum and minimum values of T both drop below their first-order values (dashed lines), because of the second-order dependence of T on irradiance (see Eq. (12)). For far-field detection ($v \approx -z/z_R$), these second-order effects have no net effect on ΔT, and so it is only the third- and higher-order effects which cause ΔT to deviate from its first-order value. Therefore, the initial slope of the middle curve (at $\Delta\Phi_0 = 0$) is 0, while for $\Delta\Phi_0 = 1$, the error in ΔT is only 0.4%. Higher-order effects are more important for the thick refractor (Fig. 8(b)). Note that nearly all of these effects are associated with $T_{\max}$ (for a positive refractive nonlinearity), which corresponds to the front (entrance) face of the sample being at the beam waist. In this situation, the self-focusing reinforces itself as the beam propagates in the medium, enhancing T. An expression for the higher order nonlinear transmittance effects has been given in Ref. 41.

Figure 8(c) shows the situation for pure nonlinear absorption, for apertureless Z-scans ($S = 1$) with thin and thick media. The thin medium result is in agreement with Eq. (2). Higher-order effects are important for lower values of the nonlinear parameter than is the case for nonlinear refraction. This is partly because ΔT is now given by $1 - T_{\min}$, and so there is no longer a cancellation of trends in $T_{\max}$ and $T_{\min}$. Another significant factor is that absorption of light in the medium reduces the irradiance available for promoting further nonlinear absorption, giving

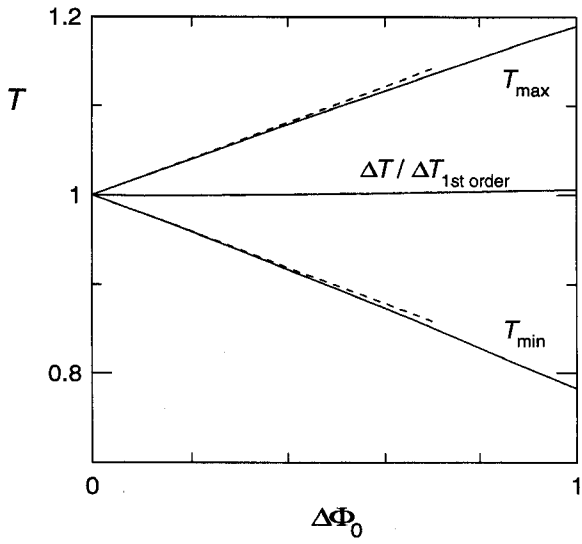

(a)

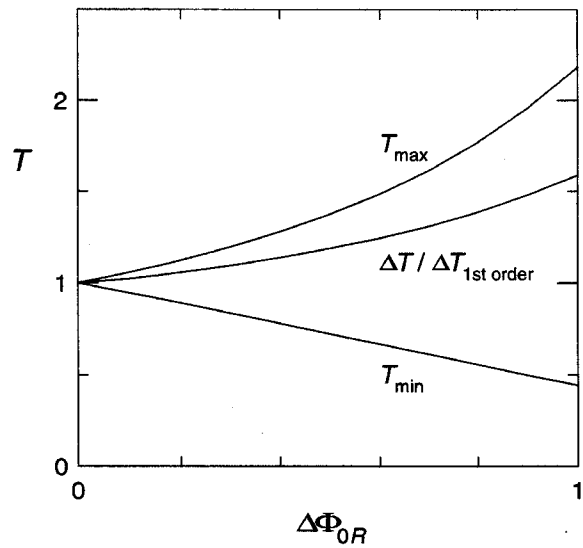

(b)

Fig. 8. Dependence of T_{max}, T_{min} and ΔT on the nonlinear phase shift ($\Delta\Phi_0$ or $\Delta\Phi_{0R}$) or the nonlinear absorption parameter (Q_0 or Q_{0R}), showing effects higher than first order in irradiance. Here $n_0 = 1.5$, $\alpha_0 = 0$; $\lambda = 532$ nm; $z_R = 2$ mm; $L = 0.1$ mm (thin) or 0.1 m (thick). (a) Thin nonlinear refractor, $S = 0.01$ (pinhole). (b) Thick nonlinear refractor, $S = 0.01$. (c) Nonlinear absorber, $S = 1$ (apertureless).

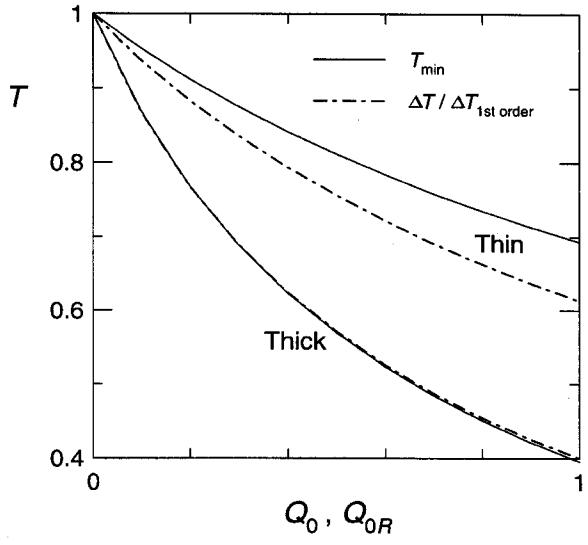

(c)

Fig. 8. (*Continued*)

rise to significant higher-order effects even for the thin sample. For a thin nonlinear absorber, the saturation of the nonlinear absorption with increasing irradiance is as described by Eqs. (2) and (21). An expression for the saturation of the nonlinearity for the thick absorber has been given elsewhere.[41]

3. Experimental Techniques and Analysis

To use the Z-scan technique intelligently and correctly, experimental conditions need to be carefully controlled. We now discuss the impact of various experimental parameters on Z-scan measurements and the subsequent analysis.

3.1. *Laser Beam Spatial Profile*

In the measurement of optical nonlinearities, the knowledge of the laser beam profile is particularly important. This is especially so for the Z-scan measurement of nonlinear refraction, which relies on measuring and analyzing induced distortions of the spatial profile of the beam. Effects with non-Gaussian beams have been considered by Hermann,[28,42] who used a parameter ν to allow for cylindrically symmetrical beam profiles including Lorentzian, Gaussian, parabolic and top-hat. Zhao *et al.*[43] investigated Z-scans of liquid crystals using a top-hat beam, and Mian and Wicksted[44] have measured the nonlinearity of a lead silicate glass using an approximately elliptical Gaussian beam.

In a subsequent analysis,[45] Mian *et al.* extended the thin medium theory to include elliptical Gaussian beams. These beams have Gaussian distributions in their semimajor and semiminor axis directions (x- and y-directions), and generally have different waist sizes and positions corresponding to the distributions in these two directions. Mian *et al.* demonstrated variations in the Z-scan profiles which occur with variations of both the ellipticity of the laser beam and the spacing between the waist positions. Under certain conditions, an additional peak appears in the Z-scan profile, which does not occur for a cylindrical Gaussian beam.

The spatial profile of a laser beam which is not necessarily Gaussian can be characterized in terms of its M^2 value as defined by Siegman.[46] The M^2 value is effectively the ratio of the divergence of the beam to the divergence of a Gaussian beam of the same waist size. For a Gaussian beam $M^2 = 1$ and for all other profiles $M^2 > 1$ in a linear medium. Accurate determination of M^2 is, in itself, a non-trivial exercise. In our Z-scan studies the beam profile was measured in both the x- and y-directions at several different positions along the z-axis. A scanning slit method was used and the measured values of the beam radii ($1/e^2$) were corrected to allow for the finite slit width.[47] The M^2 value, waist position and size were all determined by performing a three-parameter fit to the second moment of position, $< x^2 >$ or $< y^2 >$, measured at the different z positions. Using this procedure, it was possible to measure M^2 values to the necessary accuracy (2 decimal places) for reliable Z-scan results.

Modeling studies have been carried out to determine the relationship between the M^2 value and the T value. These studies used randomly generated beam profiles which were approximately Gaussian in shape, but not necessarily cylindrically symmetrical - typical of laser profiles encountered in the laboratory. The beams in the model were propagated using a fast Fourier transform technique, and nonlinear effects in thin media were incorporated. Details of these calculations are reported elsewhere[48] and will not be included here. Figure 9 shows plots of ΔT versus M^2 obtained from the modeling studies, for measurements of nonlinear refraction (using a pinhole aperture) and nonlinear absorption (no aperture). The ΔT values were normalized to the values $\Delta T_{\text{Gaussian}}$ calculated for Gaussian beams with the same waist sizes (as determined from the second moment of position).

Two overall trends were observed. Firstly, there was an increasing scatter in $\Delta T/\Delta T_{\text{Gaussian}}$ values as M^2 increased (as beam quality declined), particularly for nonlinear refraction. For this case, M^2 needs to be 1.1 or better to give less than 5% standard deviational scatter in $\Delta T/\Delta T_{\text{Gaussian}}$. We aim to have M^2 less than 1.05. For an absorptive nonlinearity, M^2 needs to be less than about 1.3 in order to provide less than 5% standard deviational scatter in $\Delta T/\Delta T_{\text{Gaussian}}$. Secondly, the value of $\Delta T/\Delta T_{\text{Gaussian}}$ increases with M^2, particularly for nonlinear absorption. The increases are related to the definition of the beam radius and the peak irradiance used to calculate $\Delta T_{\text{Gaussian}}$ (see Ref. 48). The precise nature of the trends depends somewhat on the selection of non-Gaussian beams, but the study serves to indicate the sensitivity of the Z-scan technique to beam profile irregularities. These results

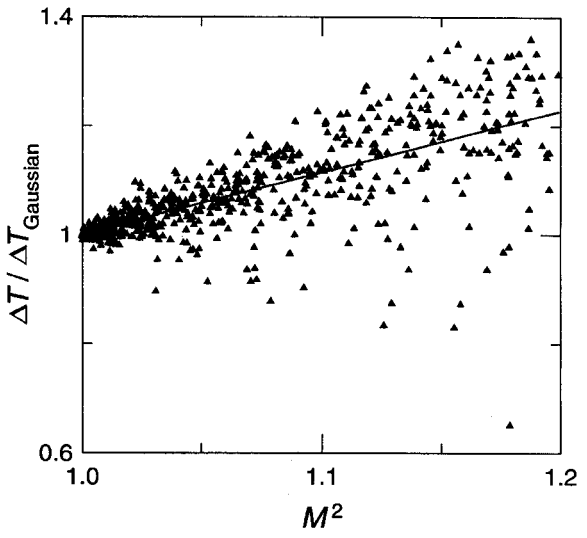

(a)

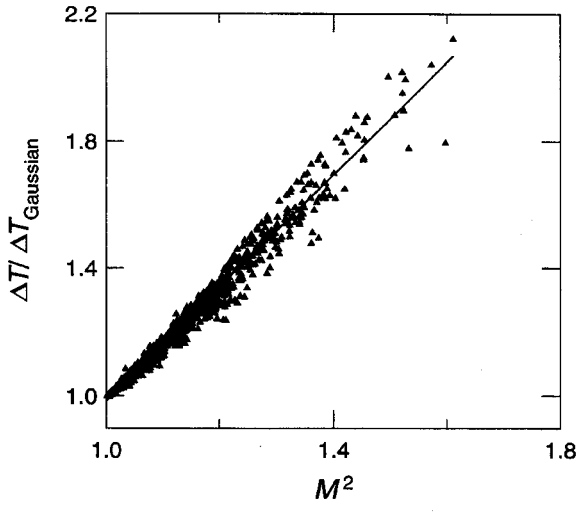

(b)

Fig. 9. ΔT versus M^2, from theoretical modeling.[48] (a) Nonlinear refraction. (b) Nonlinear absorption.

cast doubt on the validity of the technique of Agnesi *et al.*[49] for measuring beam quality by a simple application of the Z-scan technique.

Achievement of a good spatial beam profile can be a delicate task, particularly as a satisfactory profile needs to be maintained over a large range of z values.

We have found that the use of a spatial filter alone to improve beam quality is insufficient, as the aperture of the spatial filter produces diffraction rings which must be eliminated. Placement of an iris after the spatial filter to eliminate the diffraction rings has proven to be an inadequate solution, resulting in M^2 values greater than 1.05. Figure 10 is a schematic diagram of the experimental arrangement we have adopted for Z-scan measurements. Light was deflected to the reference detector using a wedge, avoiding problems caused by interference between front and back reflections from parallel-surface reflectors. The wedge was placed at the minimum deviation angle, to avoid astigmatism in the beam. The spatial filter and wedge were followed by an apodizer, which was placed immediately before the focusing lens. With this arrangement we found it was possible to obtain routinely M^2 values of less than 1.05.

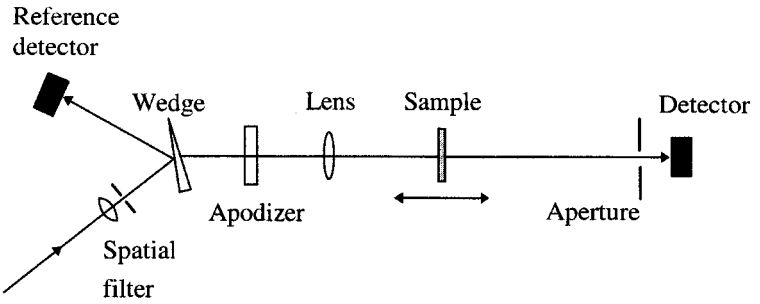

Fig. 10. Optical set-up for Z-scan measurements.

3.2. *Temporal Characteristics of The Laser Pulse*

Time-dependence is an important issue for any pulsed laser measurements of optical nonlinearities. It should be remembered that, when using cw lasers, degenerate nonlinear effects are likely to be dominated by thermal nonlinearities, a fact that has sometimes been overlooked.[50] These effects are often non-local (that is, the refractive index or absorption coefficient depends on the irradiance at a different position in the sample), and for liquid samples they may even involve convective effects, introducing asymmetry.[20,51] The nonlinear effects of this type are unlikely to be described by Eqs. (3) and (13), and blind application of the theory described here may result in measured nonlinearities which vary as the focal conditions are adjusted (see Ref. 52). This might also be of concern in pulsed laser experiments, and may be indicated by effects which depend on the repetition rate of the laser. In this instance, the repetition rate should be reduced until all the nonlinear effects are observed to be independent of repetition rate, before the theory described in this paper can be applied.

When the response time of the nonlinearity is much shorter than the laser pulse width, the nonlinear effect may be assumed to depend on the instantaneous

irradiance in the sample. While time-resolved measurements are possible,[53] it is generally more convenient to measure pulse energies than instantaneous powers, and a better signal to noise ratio can be obtained in this way. When the nonlinear transmittance is measured using pulse energies, there must be time integration of the equations, taking account of the recorded pulse shape. For a temporally Gaussian pulse of irradiance $I(t) = I(0)\exp(-t^2/\tau^2)$ and an instantaneous nonlinear transmittance $T(t) = 1 + T^{(1)}I(t) + T^{(2)}I(t)^2 + \ldots$, the effective nonlinear transmittance is related to the peak irradiance $I(0)$ by the expression

$$T_{\text{effective}} = \frac{\int T(t)I(t)dt}{\int I(t)dt} = 1 + \frac{T^{(1)}I(0)}{\sqrt{2}} + \frac{T^{(2)}I(0)^2}{\sqrt{3}} + \ldots . \tag{41}$$

Accurate determination of fast nonlinearities with a pulsed laser relies on being able to relate the peak power accurately to the measured pulse energy. A single longitudinal mode is necessary, or at least a reliable and well-characterized pulse shape. For a temporally Gaussian pulse of power $P(t) = P(0)\exp(-t^2/\tau^2)$, the full width at half-maximum (FWHM) pulse length is $2\tau/\sqrt{(\ln 2)}$ and the pulse energy is $P(0)\tau\sqrt{\pi}$. Equation (41) can be used to relate the measured Z-scan result to the nonlinearity of the medium.

Assuming that the pulse is temporally Gaussian is generally inadequate, however, and it is therefore necessary to record the temporal profile of the pulse. Figure 11 illustrates this point. This shows a typical temporal profile of a 6.54 ns pulse from a frequency-doubled, single longitudinal mode, Nd:YAG laser, recorded using a vacuum photodiode having a response time of 100 ps. Also plotted in Fig. 11 for comparison is a Gaussian-shaped pulse of the same peak amplitude and FWHM. Note that the measured temporal profile is very close to a Gaussian shape, except

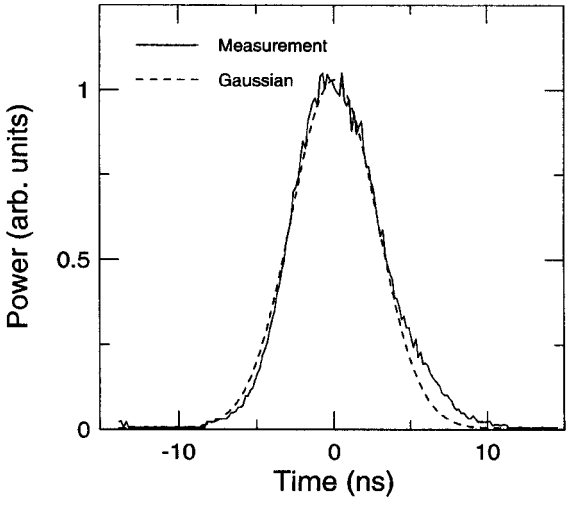

Fig. 11. Measured pulse-shape of the laser.[36]

for a small deviation at the tail of the pulse. The relationship between the peak power and the energy may be determined by comparing the time-integral of the power with the maximum power. The energy calculated from the integrated experimental profile in Fig. 11 is approximately 5% greater than the energy of the Gaussian pulse. This indicates the magnitude of the error which may be introduced by inadequate analysis of the pulse profile to obtain the value of the peak power.

Nonlinear effects are normally more greatly influenced by variations in the peak power than by variations at the lower powers in the temporal wings of the pulse. When the pulse is decidedly non-Gaussian, time-integration must be performed explicitly, and Eq. (41) is inapplicable. This is also the case when the nonlinear response is not instantaneous,[54] owing to thermal or other fluence-dependent nonlinearities.

When the nonlinear response time is much longer than the pulse width, the effects may be assumed to be fluence-dependent rather than irradiance-dependent. Many of the principles discussed in this paper are still applicable, but care must be taken to ensure that the concerns outlined in the first paragraph of this section are adequately addressed.

3.3. *Laser Power Fluctuations*

The effects of fluctuations in the laser power can normally be eliminated by dividing the transmitted power or energy by the power or energy at the reference detector (Fig. 10). This technique produces a much cleaner-looking Z-scan trace. With optically nonlinear samples, however, the relationship between the input laser power and the power measured at the signal detector is complicated (and often unknown) making this correction of the data inadequate when the laser power varies by more than a few percent. In Z-scan measurements, fluctuating laser power is manifested as a randomness in the data curves and is reminiscent of noise.

One method for overcoming this deficiency is to record data at each point only when the input power falls within well-defined limits. This method is demonstrated in Fig. 12, which shows results from an apertureless Z-scan of a platinum ethynyl compound dissolved in tetrahydrofuran, exhibiting nonlinear absorption.[55] These measurements were made using an active-passive mode-locked, 20 ps, 1064nm laser. In this case the input power varied by approximately 50% during the scan, producing noisy and inaccurate data. Employing data restriction, the recording of data took place only when the input power was within 2.2% of the mean value, resulting in a much improved profile. The advantages of employing this data restriction method are even more noticeable when the laser is highly unstable or when the nonlinear process has a sharp energy threshold. It should be noted that the residual randomness displayed in the restricted data of Fig. 12 was caused by laser induced scattering in the sample.

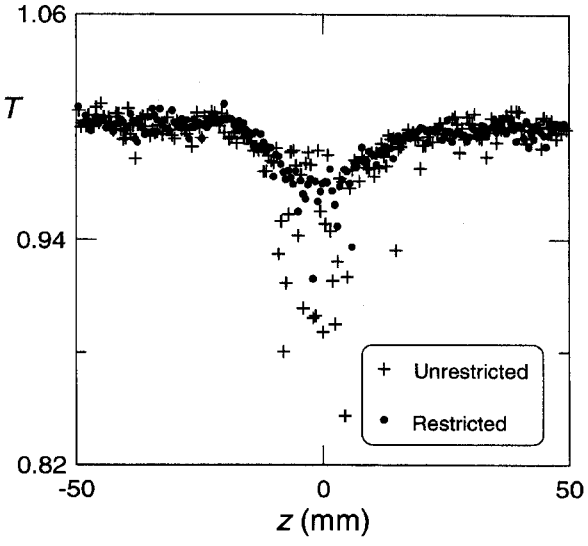

Fig. 12. Noisy Z-scan profile of platinum ethynyl solution,[55] showing the advantages of data restriction.

3.4. *Etalon Effects in Non-Ar-Coated Samples*

Problems can arise with samples which have not been anti-reflection coated since they form low-finesse Fabry-Perot etalons. The transmission of a lossless Fabry-Perot is described by the well-known equation

$$T_{\mathrm{FP}} = \frac{1}{1 + F\sin^2(\phi/2)}, \tag{42}$$

where ϕ is the double-pass phase shift given by $\phi = 4\pi n_0 L/\lambda$, and F is the coefficient of finesse, which is related to the surface reflectance R and the finesse F' by

$$F = \frac{4R}{(1-R)^2} = (2F'/\pi)^2 . \tag{43}$$

For an uncoated sample with light moving from refractive index n_i to n_0 (at normal incidence to the interface), the reflectance is

$$R = \left(\frac{n_0 - n_i}{n_0 + n_i}\right)^2 . \tag{44}$$

Assuming a reflectance of 4% ($n_i = 1, n_0 = 1.5$), one observes that there is a maximum possible change in transmission of 15% (from the maximum value of 1 to a minimum value of 0.85) when parameters such as the sample length or refractive index of the medium vary. Reduction of the maximum possible modulation to less than 1% requires that the surface reflectivity be less than 0.25%.

We have observed temporal variations in the transmission of liquid samples caused by changes in the sample temperature. These changes altered the optical path length, $n_0 L$, resulting in the transmission variation predicted by Eq. (42). By using ar-coated cells to contain the liquid, these transmission variations were avoided. (The internal interface between the cell wall and the liquid had a surface reflectivity of around 0.2%, which produced no noticeable effect.)

In addition to unwanted transmission variations in uncoated samples, reflections vary the irradiance within the sample, upsetting the measurement of the nonlinearity. Reflection effects in a self-focusing medium have been examined in some detail by Sutherland,[56] who used the aberrationless approximation in his analysis. This approach does not accurately take account of the shape of the beam in the medium, particularly under the influence of surface reflections, but it does give an indication of the consequences of these reflections. For low nonlinear phase shifts ($\Delta\Phi_0 \approx 0.01$), the reflectance R enhances the nonlinear phase shift within the sample by a factor $(1 + R)/(1 - R)^2$, when the cavity is in resonance with the laser wavelength. For low reflectance and moderate phase shift ($R = 6.7\%$, $\Delta\Phi_0 = 0.5$), the nonlinear phase shift can push the cavity towards or away from resonance, destroying the symmetry of the Z-scan profile. For moderate reflectance and large nonlinear phase shifts ($R \approx 50\%$, $\Delta\Phi_0 = \pi$), strong feedback effects such as optical switching and bistability can take place.

Michelotti *et al.*[57] have experimentally investigated the role of surface reflections on Z-scan profiles, using an InSb sample and a CO_2 laser at a wavelength of 10.6 μm. They observed asymmetrical profiles and other distortions of the profiles caused by resonance effects, consistent with numerical solutions of a nonlinear Fabry-Perot resonator model.

For reliable Z-scan measurements, it is recommended that at least the rear surface of the samples be ar-coated, in order to remove etalon effects and uncertainty about the field. This is particularly so in the case of high refractive index material, if detailed numerical modelling and fitting of parameters are to be avoided.

3.5. *Sample Thickness — How Thin is Thin?*

In general, Z-scan studies are carried out with "thin samples," which allows the data to be analyzed using Eq. (1) or (2). Thin sample analysis is only approximate, however, since it fails to take account of diffraction-induced changes in the beam profile as the beam propagates through the sample.

The validity of thin sample analysis requires that the sample length L be much shorter than the Rayleigh length z_R, which is a measure of the distance scale over which the beam profile changes. In the presence of nonlinear refraction, the beam profile can change over a shorter distance scale, giving rise to the additional requirement $L \ll z_R/|\Delta\Phi_0|$ when $|\Delta\Phi_0|$ is larger than 1. The question arises as to whether samples used in experiments adequately meet these thin sample criteria.

Figure 13(a) shows the variation in ΔT with sample thickness for a nonlinear refractor, evaluated using Eq. (30). Here ζ_m is the thickness, normalized to the Rayleigh length within the medium, $n_0 z_R$. As the sample length increases, ΔT declines in proportion to the thin sample value, and is 94% of this value when $\zeta_m = 1$.

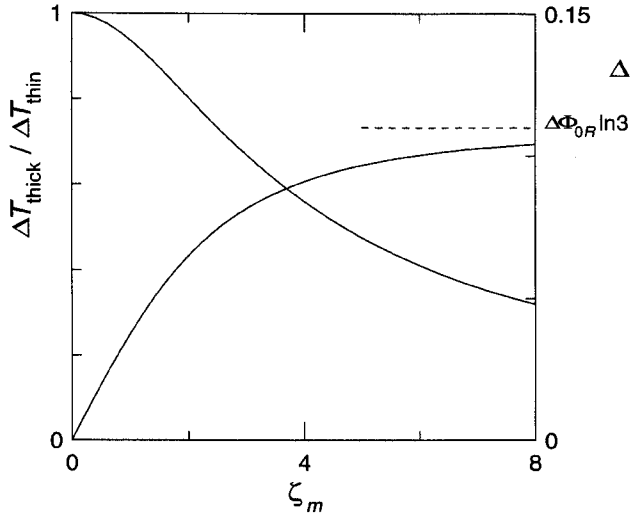

(a)

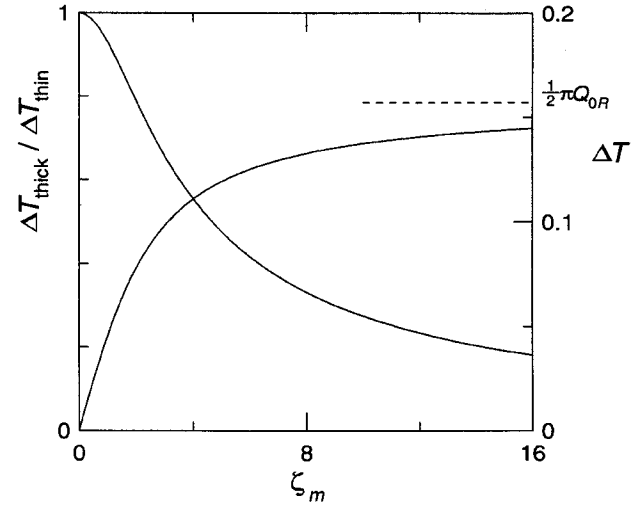

(b)

Fig. 13. ΔT as a function of sample thickness, to the first order in irradiance. (a) Nonlinear refraction (pinhole), $\Delta\Phi_{0R} = 0.1$. (b) Nonlinear absorption (apertureless), $Q_{0R} = 0.1$.

If samples as long as this are used, it is important to correct for the sample thickness. Note that ΔT reaches 90% of its ultimate value ($\Delta\Phi_{0R} \ln 3$) when $\zeta_m = 5.6$; ie. when the sample length is approximately six Rayleigh lengths. This is important for the design of optical power limiters. This behavior has also been found to apply when higher-order effects are significant, and the 90% value for ΔT at $\zeta_m \approx 6$ has been verified experimentally within the strongly nonlinear regime.[36]

Figure 13(b) shows the analogous situation for a nonlinear absorber. In this case, the ΔT value drops to 93% of the thin medium value when $\zeta_m = 1$. A longer sample is required to saturate the nonlinearity in the weak interaction regime: $\zeta_m = 12.6$, to achieve 90% of the maximum absorption $\left(\frac{1}{2}\pi Q_{0R}\right)$. In the strongly nonlinear regime, the saturation length is much shorter, becoming shorter with increasing optical power.

3.6. *Aperture Size — When is an Aperture a Pinhole?*

In the measurement of refractive nonlinearities using the conventional Z-scan technique, the far-field aperture is normally a pinhole, ensuring measurement of only the on-axis transmission. A question which naturally arises is, "When is an aperture a pinhole?" This may be determined experimentally by choosing successively smaller pinholes until the transmission characteristics are essentially independent of the pinhole size. Alternatively, translation of the aperture in the x- or y-direction by a distance of one or two aperture diameters will produce no change in signal if the aperture is a true pinhole. A more satisfactory method of answering the question is to address the problem analytically.

Equation (26) gives the nonlinear transmittance as a function of S, the linear transmittance of the aperture. Through appropriate manipulation of this equation it is possible to derive an approximate expression which corrects the ΔT value to accommodate finite apertures. For the case of a purely refractive nonlinearity, we find:[28]

$$\Delta T(S) \approx (1 - S)^{0.268} \Delta T(S = 0)\,. \tag{45}$$

The correction factor in this equation agrees closely with the factor $(1 - S)^{0.25}$ obtained empirically by Sheik-Bahae *et al.*[2] These equations assume that the z-values of the maximum and minimum are $\pm 0.8585 z_R$, which is true for the case of a pinhole aperture in the far-field. This simple assumption breaks down for larger values of S, however, and it is necessary to resort to numerical techniques to assess the aperture correction factor, which is plotted in Fig. 14. For small apertures ($S < 0.2, r_a/w < 0.33$), there is good agreement between the numerical and analytical results, and it is possible to estimate the variation in ΔT brought about by a finite aperture using Eq. (45). Inserting a value of $S = 0.01 (r_a/w = 0.07)$ gives a correction factor of 0.997, revealing that an aperture having a linear transmittance of 1% is a good approximation to a pinhole.

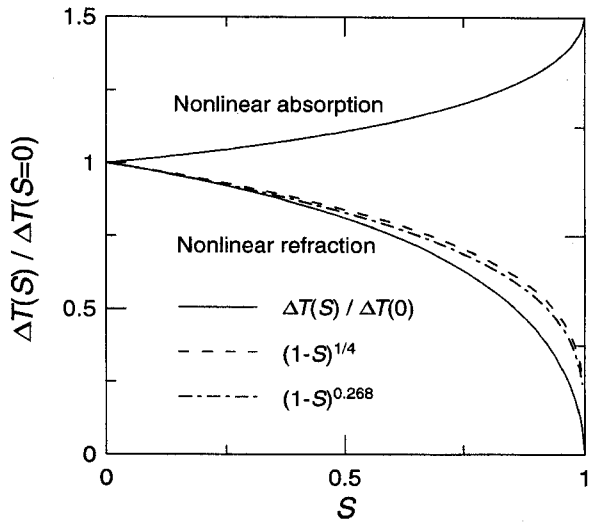

Fig. 14. ΔT as a function of aperture parameter S.

For a purely absorptive nonlinearity and far-field detection ($v = -z/z_R$), Eq. (26) provides the result

$$\Delta T(S) = \frac{3}{2S}[1 - (1 - S)^{2/3}]\Delta T(S = 0)\,, \tag{46}$$

which is also plotted in Fig. 14. Note that the ΔT value in the nonlinear absorption case is actually smaller for a pinhole than it is for a larger aperture (or no aperture). This is because the absorption close to the beam axis tends to cause a bright diffraction spot on-axis in the far-field, partially countering the absorption-induced reduction in irradiance. For an S value of 0.01, the correction factor is 1.002, indicating that an aperture with a linear transmittance of 1% is again a very good approximation to a pinhole also for an absorptive nonlinearity.

3.7. *Aperture-Waist Distance — Where is the Far Field?*

As the Z-scan method for refractive nonlinearities measures induced spatial distortions in the far field, an important experimental parameter is the distance z_1 from the beam waist to the aperture and signal detector. The variation of ΔT with z_1 may be evaluated to first order by differentiating Eq. (11) with respect to z. When z_1 is finite, the maximum and minimum are both increased from their far-field values. For a distance of 10 Rayleigh lengths, the maximum is increased by around 18% (for a small positive refractive nonlinearity); at 20 Rayleigh lengths, the amount is 9%. Because the minimum is also increased, the effects on ΔT largely cancel one another.

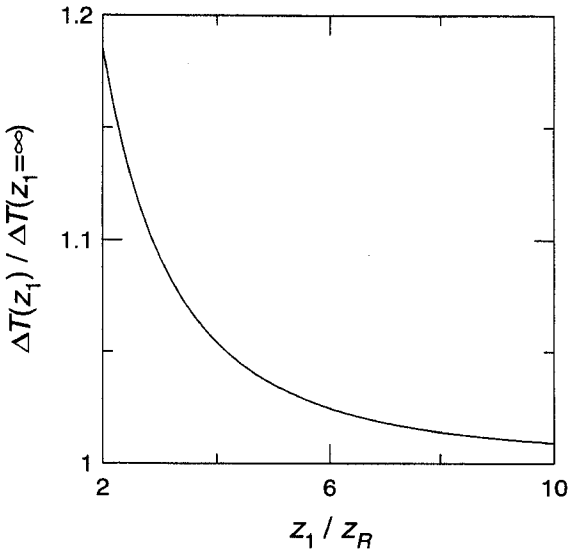

Fig. 15. ΔT as a function of observation plane position z_1.

The results for ΔT are shown in Fig. 15. For values of z_1 greater than $2z_R$, we have found these results to be well approximated by the empirical formula

$$\frac{\Delta T(z_1)}{\Delta T(\infty)} \approx 1 + \frac{0.9}{0.8 + (z_1/z_R)^2} \,. \tag{47}$$

For a distance of 10 Rayleigh lengths to the observation plane, ΔT is 1% greater than the corresponding value at infinite distance. Increasing the distance to 20 Rayleigh lengths decreases the variation to 0.2%. From these results it would seem that a reasonable approximation to the far field is a distance of 10 Rayleigh lengths or more, *provided we are concerned only with determining the* ΔT *value.* In the case of tight focusing where the Rayleigh length of the focused beam is 1 mm or less, placement of the aperture and signal detector at a distance which is truly representative of the far field should pose no practical difficulties. For weakly focused beams it may be necessary to tolerate inaccuracies of greater than 1% to accommodate a practical experimental arrangement, or preferably to use Eq. (47) to correct measured values.

3.8. *Aperture Alignment*

In the measurement of nonlinear refraction, the pinhole or aperture must be centered on the optical axis of the laser beam which exits the sample. This is normally accomplished by moving the pinhole in both the x- and y-directions to maximize the signal in the linear (low irradiance) regime. The question arises: how important is the accurate alignment of the pinhole? Again, the discussion will be restricted to refractive nonlinearities ($\alpha_I = 0$), because normally apertures are not used in measurements of nonlinear absorption. The situation in which refractive and absorptive

nonlinearities are both present is readily modeled using the equations presented in Sec. 2.3.

The effects of misalignment can be calculated using Eq. (23), which is correct to the first order in irradiance. Z-scan profiles look quite different when the pinhole is sufficiently far away from the axis. When nonlinear refraction enhances the on-axis irradiance in the far field, it naturally reduces the irradiance in the wings, interchanging the profile's peak and dip.

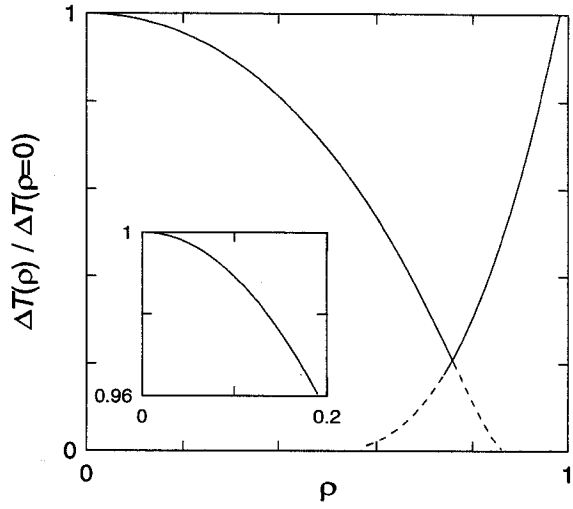

Fig. 16. ΔT as a function of pinhole misalignment parameter ρ.

Figure 16 shows the dependence of ΔT on the aperture misalignment parameter ρ (the radial displacement normalized by the beam size at the observation plane). For ΔT to agree with the on-axis result to within 1%, ρ must be less than 0.1. In practice, the pinhole is normally centered by moving it in the x- and y-directions to optimize its transmission in the linear regime. For a Gaussian-shaped beam, a ρ value of 0.1 corresponds to a 2% drop in pinhole transmission. If the pinhole displacement is such that the linear transmission is reduced by 5%, the error in ΔT is 3%. This illustrates the care that must be taken in positioning the pinhole for an accurate determination of nonlinearities.

When the beam profile is asymmetrical or otherwise distorted, the optimal position of the pinhole is difficult to determine. The normal laboratory practice is probably to place the pinhole at the position which maximizes the throughput in the linear regime. This criterion was taken into account in the calculations of ΔT values for the plots of Fig. 9, for irregular beam profiles.

It is interesting to note that $\Delta T(\rho)/\Delta T(\rho = 0)$ increases rapidly with ρ, when ρ is greater than 1. This feature has been exploited in the so-called EZ-scan[22–24]

and other methods using the off-axis irradiance to enhance the sensitivity of the Z-scan technique. These methods will be discussed in Sec. 3.10.

3.9. *Sample Imperfections*

The Z-scan technique relies on scanning a sample along the z-axis while measuring variations in transmittance caused by the optical nonlinearities. Sample imperfections produce variations in the transmittance which are not caused by optical nonlinearities. They make the measurement process more difficult, and can even obscure the nonlinear effect. This problem is particularly important for nonlinear refraction measurements, since beam steering by the sample affects the amount of light entering the aperture or pinhole.

Insertion of a sample which is wedged will steer the laser from the intended direction of propagation, effectively making the pinhole off-axis. We have modeled this effect using Eq. (23), to ascertain the effects upon Z-scan measurements, and we have determined a method for aligning the pinhole to minimize these effects. Wedging can be incorporated by expressing the radial position r as a function of the sample z-position and the beam deflection angle θ_w produced by the wedged sample:

$$r = \theta_w(z_s - z)\,. \tag{48}$$

Here z_s is the value of z for which the pinhole's x-y position is optimized ($r = 0$). While T has been defined as the transmittance normalized to the linear transmittance of the sample, in the case of an imperfect sample this linear transmittance must be defined at a particular value of z. We have chosen $z = z_s$.

Figure 17 shows the results of this modeling. Figure 17(a) simulates the condition where the x-y position of the aperture has been optimized with the sample located at the initial position of the scan ($z_s = -10$ mm). Figure 17(b) shows the result when the x-y position of the aperture has been optimized with the sample placed at the center of the scan range. Included in each figure is the predicted profile when the sample has no nonlinearity ($n_I = 0$) and the predicted profile of a perfect (unwedged) sample. From these results it can be clearly seen that the best profile and most accurate value of T will be obtained when x-y alignment of the aperture is carried out with the sample placed at the center of the scan range. Nevertheless, wedge effects are still present.

Another situation that arises is the presence of lens effects in the sample. Figure 18 shows an interferogram of a commercially available glass cell containing carbon disulfide. The interference fringes show clearly distortions caused by wedge and lens effects in the cell. We have modeled lens effects by ascribing a focal length F to the sample. While this obviously does not cater fully for cell astigmatism and other aberrations, it illustrates the consequences of lensing, and allows lens and wedge effects to be incorporated simultaneously using a modified version of Eq. (23). The lensing of the sample affects the value of v,[30] and it also affects the beam radius $w = w(z_1, z)$ in the linear regime.

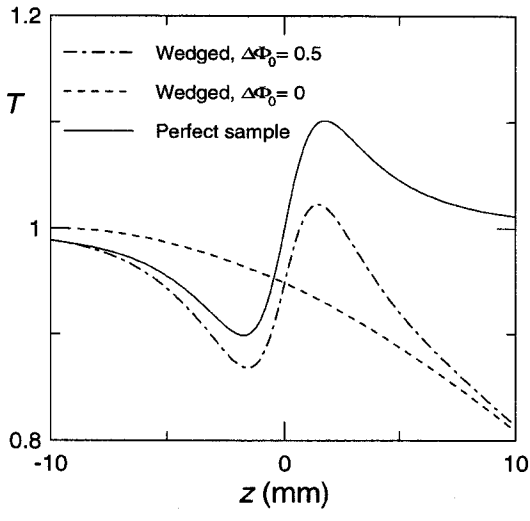

(a)

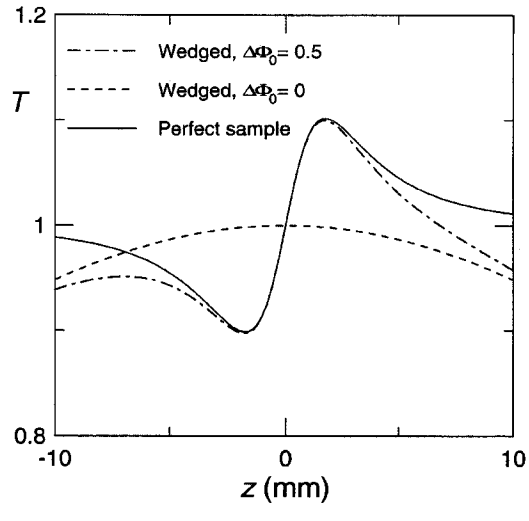

(b)

Fig. 17. Z-scan results for wedged nonlinear samples, with $\theta_w = 1.5$ mrad, for different values z_s of the sample position for aligning the pinhole. (a) $z_s = -10$ mm. (b) $z_s = 0$.

The relevant equations are:

$$\frac{I(r, \Delta\Phi_0, z)}{I(0,0,0)} = \frac{w(z_1,0)^2}{w(z_1,z)^2}\left\{ \exp(-2\rho^2) + \frac{2\Delta\phi_0}{9+v^2}[(3+v^2)\sin\Psi - 2v\cos\Psi]\exp\left[\frac{-4\rho^2(3+v^2)}{9+v^2}\right]\right\} \tag{49}$$

Fig. 18. Interferogram showing distortions in commercial glass cells containing CS_2.

where

$$v = -\frac{1}{z_R}\left(z + ({z_R}^2 + z^2)\left(\frac{1}{z_1 - z} - \frac{1}{F}\right)\right),$$

$$\frac{w(z_1, z)^2}{{w_0}^2} = \frac{(1+v^2)(z_1 - z)^2}{{z_R}^2 + z^2},$$

$$\rho = r/w(z_1, z)$$

and

$$\Psi = 8\rho^2 v/(9 + v^2).$$

Figure 19 shows the results of modeling a sample with lensing ($F = 0.5$ m). In this case, the value of z_s is irrelevant, since lensing alone does not steer the beam away from the optic axis in this model. The linear result ($\Delta\Phi_0 = 0$) has a positive slope, which is to be expected for a negative lens or for a positive lens when the distance from the sample to the pinhole (10 m in this case) is greater than the focal length of the lens. Equation (49) can also be used to calculate Z-scan results when wedge and lens effects are both present.

Scratches and sample roughness also affect the outcome of Z-scans. This has been modeled by McDuff,[38] who used a statistical approach to generate random, uncorrelated phase irregularities with mean $\langle\phi\rangle = 0$ and variance $\langle\phi^2\rangle = (\delta\phi)^2$. Figure 20 shows a Z-scan of a roughened nonlinear refractor with $\delta\phi = 0.05$, for two different power levels, together with the regular sample Z-scan. When the phase irregularities are comparable with or greater than the nonlinear phase change, the Z-scan profile becomes barely recognizable.

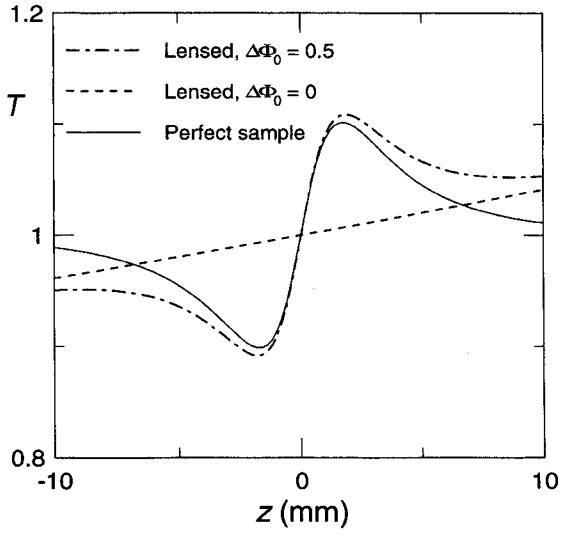

Fig. 19. The effects on Z-scan of lensing in nonlinear samples ($F = 0.5$ m).

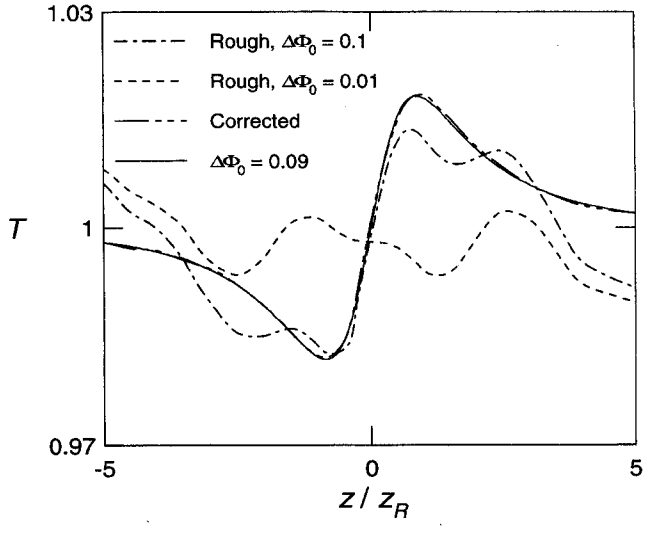

Fig. 20. Modeled Z-scans of a roughened sample at high and low powers, showing the use of subtraction to obtain a corrected profile.

Sheik-Bahae *et al.*[2] have advocated a method of correcting for sample irregularities, which involves subtracting the linear background from the nonlinear measurement of T, and adding 1. Results of this correction are shown in Fig. 21, for the wedged sample data of Fig. 17. Note that the best results are obtained when $z_s = 0$,

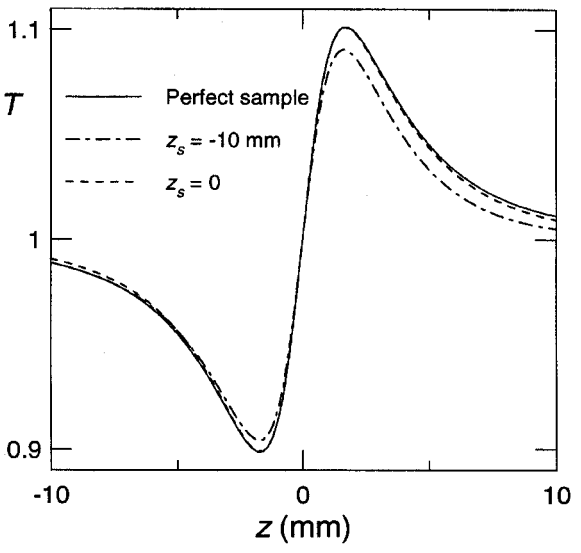

Fig. 21. Corrected Z-scan traces for the wedged sample data of Fig. 17.

that is, the pinhole's x-y position should be optimized when $z = 0$. Correction of the data for the lensed sample (Fig. 19) results in very good agreement with the perfect sample curve.

In practice, it is often difficult to reduce the laser power to a level at which there is no nonlinearity, without adversely affect the signal-to-noise ratio. It is then better to measure T at both a high power and low power, and to relate the transmittance difference to the difference in powers. This method is used in the corrected Z-scan profile for the roughened sample data in Fig. 20. This profile approximates well the perfect sample profile for $\Delta\phi_0 = 0.09$. Correction of real Z-scan data which we obtained using a thick sample is shown in Fig. 22.

3.10. *Extensions of Z-Scan*

The Z-scan technique has been modified or extended in several ways to increase the scope of its usefulness. One of these approaches is the eclipsing Z-scan[22–24] (EZ-scan), which enables one to increase the sensitivity by a large factor, by monitoring the power delivered to positions removed from the optical axis. In the case of a nonlinearly refracting sample, a reduction in the far-field on-axis irradiance corresponds to an increase in the irradiance away from the axis. As indicated in Fig. 16, by monitoring at a sufficient distance from the optical axis ($\rho > 1$), high sensitivities to the nonlinearity can be achieved. This approach is particularly useful for measuring weak nonlinearities or when using very thin samples, for which the signal-to-noise ratio is low, and also when optical damage problems necessitate measurements at low irradiances.

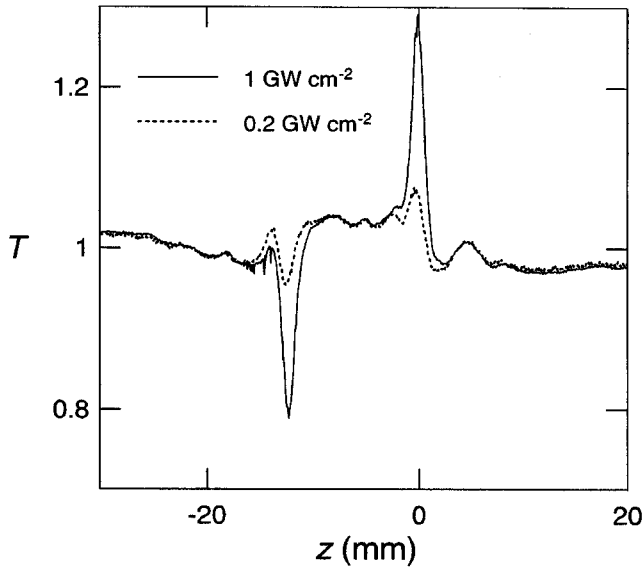

(a)

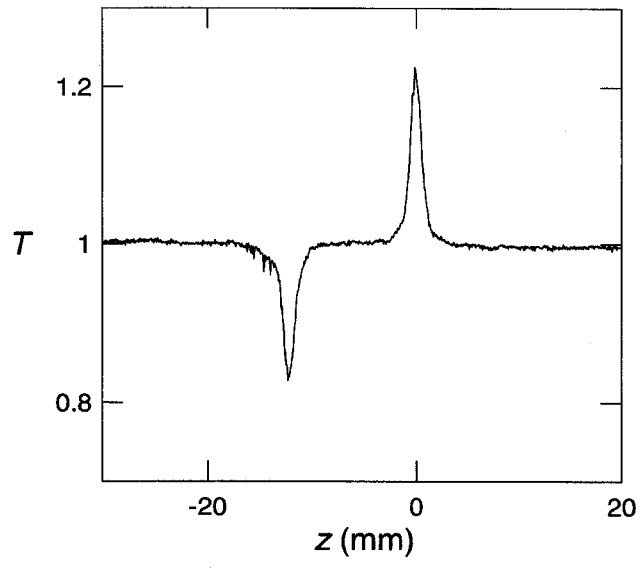

(b)

Fig. 22. Correction of real Z-scan data,[36] for a 20 mm cell of CS_2. (a) Raw data for high and low powers (waist irradiances indicated). (b) Corrected data, from subtraction of the curves in (a).

In the EZ-scan technique, the central portion of the beam is blocked at the far-field by a circular disk. For a Gaussian-shaped laser beam, the linear transmittance of the disk block is now $1 - S$, with S having been computed by Eq. (25). Xia *et al.*[23] have given an empirical relationship for ΔT with a nonlinear refractor and a small nonlinear phase shift ($|\Delta\Phi_0| < 0.2$):

$$\Delta T \approx 0.682(1 - S)^{-0.443}|\Delta\Phi_0| . \tag{50}$$

The larger the disk radius, the greater the EZ-scan sensitivity becomes, although clearly the disk size must be limited by the need to transmit sufficient light for a reliable measurement. Xia *et al.* have used the value $S = 0.99$, which corresponds to a disk with a radius which is 1.52 times the $1/e^2$ beam radius.

A difficulty with the EZ-scan method is that for an imperfect non-Gaussian beam, the wings of the beam are likely to be considerably distorted, so that Eq. (50) is no longer valid. The larger the value of S, the more serious this problem becomes. This creates uncertainty in the measured nonlinearity when the beam quality is not ideal. This concern does not necessarily detract from the use of the technique with lower quality beams for comparing a test sample with a reference sample, as advocated by Xia *et al.*[22] and Bridges *et al.*[21]

Along similar lines to the EZ-scan, Tian *et al.*[58,59] have suggested the use of an off-center aperture to enhance the Z-scan sensitivity. The same beam quality considerations apply to this case. It should be emphasized that, if off-axis detection is to be used, the same detection geometry should be used in the reference detector arm of the experiment (see Fig. 10). This will reduce the problems caused by variations in the laser profile and beam-pointing instability. This approach is shown in the diagrams of Xia *et al.*, but not those of Tian *et al.*

In a further development, Marcano *et al.*[60] used a CCD camera to monitor the entire far-field beam distribution. It appears that the resolution in the transmittance measurement was considerably limited by noise and the 8-bit resolution of the CCD camera.

The Z-scan technique has been used with different laser polarization conditions,[61,62] to obtain information about the different tensor components of $\chi^{(3)}$. In one of these studies,[61] the sample was positioned successively at the z-positions corresponding to the minimum and maximum of the Z-scan profile, while the angular orientation of a polarization analyzer was varied. In a similar way, temporal information about nonlinearities has been obtained by positioning the sample at the minimum and maximum positions and recording the time-dependence of the transmittance.[53]

A reflection Z-scan technique has been investigated by Petrov *et al.*[63,64] for studies of highly absorbing samples. The beam reflected by the sample is projected through an aperture to the detector. This technique and further extensions such as the two-beam or two-color Z-scan[65–67] are beyond the scope of the present paper.

4. Conclusion

The Z-scan technique for measuring optical nonlinearities has been analyzed and discussed in detail. Experimental parameters affecting Z-scan measurements have been examined. Requirements for high beam quality and temporally characterized lasers have been given, and the need for low sample reflectivity discussed. Requirements for sample thickness, sample quality and aperture positioning have all been given. Methods for correcting non-optimal conditions have been suggested. This paper will assist experimentalists performing Z-scan measurements and will be of interest to those seeking to model or develop optical power limiters.

Acknowledgment

We wish to acknowledge the computing assistance of Peter Wilson in support of this work.

Appendix. Units and Numerical Conventions

The number of conventions for discussing nonlinear optical phenomena is quite bewildering. These aspects are discussed in some detail by Boyd[68] and by Hutchings *et al.*[69] There are several factors that contribute to this.

Firstly, we use E or $E(\omega)$ to represent the complex amplitude of the electric field within the medium (taken to be $1/\sqrt{n_0}$ times the vacuum field amplitude). The time-dependent field is

$$E(t) = \mathrm{Re}[E(\omega)e^{-i\omega t}] = \frac{1}{2}[E(\omega)e^{-i\omega t} + \mathrm{c.c.}]\,. \tag{A1}$$

Some other authors write

$$E(t) = E(\omega)e^{-i\omega t} + \mathrm{c.c.}\,. \tag{A2}$$

With this convention, the factor $1/2$ in Eq. (3) must be replaced by 2. Furthermore, expressions for nonlinear polarizations $P^{NL}(\omega)$ in terms of the driving fields are altered. While we would write

$$P^{NL}(\omega) = \frac{3}{4}\chi^{(3)}(\omega,\omega,-\omega)|E(\omega)|^2E(\omega)\,, \tag{A3}$$

those using the other convention write

$$P^{NL}(\omega) = 3\chi^{(3)}(\omega,\omega,-\omega)|E(\omega)|^2E(\omega)\,. \tag{A4}$$

This difference of conventions does not affect the values of $\chi^{(3)}$, when Eqs. (A3) and (A4) are interchanged in this way. Other authors, however, use Eq. (A4) while using the form of Eq. (A1) to describe the electric field and the nonlinear polarization. Their values of $\chi^{(3)}$ are a factor of 4 smaller than those given here.

Further differences arise because some authors would not use the factor 3 in Eqs. (A3) and (A4). The 3 arises because there are three different permutations

of the arguments of the nonlinear susceptibility $\chi^{(3)}$. Those who do not use this convention would define the nonlinear susceptibility to be three times greater.

Confusion still arises because nonlinear susceptibilities are sometimes expressed in SI (MKS) units and sometimes (more commonly) in Gaussian (esu) units. The electric field expressed in SI units (Vm^{-1}) is numerically $c(\mathrm{ms}^{-1}) \times 10^{-4}$ times its value in esu. In Gaussian units, the electric field amplitude and irradiance or intensity are related by

$$I = \frac{n_0 c}{8\pi}|E(\omega)|^2 \tag{A5}$$

(using the numerical convention of (A1)), whereas for SI units, the equation is

$$I = \frac{1}{2}\varepsilon_0 n_0 c|E(\omega)|^2\,, \tag{A6}$$

where $\varepsilon_0 = 8.8542 \times 10^{-12}\ \mathrm{Fm}^{-1}$, which is numerically equal to $10^7/(4\pi c^2)$. The use of SI units often results in a factor of ε_0 appearing on the right-hand side of Eqs. (A3) and (A4). When this is the case,

$$\chi^{(3)}(\mathrm{SI}) = 160\pi^2\varepsilon_0\chi^{(3)}(\mathrm{esu})\,. \tag{A7}$$

When there is no factor ε_0 in Eqs. (A3) and (A4), the ε_0 in Eq. (A7) should be replaced by ${\varepsilon_0}^2$.

Many authors write four arguments for $\chi^{(3)}$; the first one being the sum of the other three or the negative of that sum. This first argument is omitted here, for brevity.

Frequently, calculated molecular nonlinearities are expressed in terms of molecular hyperpolarizabilities. The total nonlinear polarization $P(\omega)$ may be related to the hyperpolarizability $\gamma(\omega,\omega,-\omega)$ of the molecules causing the nonlinearity, by taking into account local field effects.[68,70] The relevant equation for N molecules per unit volume is

$$\chi^{(3)}(\omega,\omega,-\omega) = \frac{1}{81}({n_0}^2+2)^4 N\gamma(\omega,\omega,-\omega)\,. \tag{A8}$$

We should bear in mind that the nonlinearity of a solution of nonlinear optical molecules may in general depend on the concentration and the solvent, because of intermolecular interactions, but Eq. (A8) provides a good indication of the overall nonlinearity.

In the discussion of thick nonlinear samples, Hermann and McDuff[35] use parameters α and β, which are equivalent to Q_{0R} and $2\Delta\Phi_{0R}$ in the present paper; the product $n_s n_0$ there corresponds to n_I here, and the Rayleigh length z_r there is equal to $n_0 z_R$ in the present paper.

It is appropriate at this point to mention an error in Ref. 36. In Eq. (2) is incorrect and contains an extra factor of n_0. It should read

$$\beta = 2k\gamma I_0 z_r n_0 = k n_2 {E_0}^2 z_r\,.$$

Here E_0 is the vacuum value of the electric field amplitude, whereas in the present paper E is the electric field amplitude within the sample, which is reduced by a factor of $\sqrt{n_0}$. The Rayleigh length z_r is the same as z_R in the present paper. The quantity β is equal to $2\Delta\Phi_{0R}$ in the present paper, and bears no relation to the β used by other authors to represent the nonlinear absorption coefficient, which we have called α_I.

References

1. M. Sheik-Bahae, A. A. Said and E. W. Van Stryland, *Opt. Lett.* **14**, 955–957 (1989).
2. M. Sheik-Bahae, A. A. Said, T.-H. Wei, D. J. Hagan and E. W. Van Stryland, *IEEE J. Quantum Electron.* **26**, 760–769 (1990).
3. A. L Smirl, T. F. Bogess, T. F Dubbard, J. Dubard and A. G. Cui, *Proc. SPIE* **1307**, 251–262 (1990).
4. S. Guha, S. Buchner, K. Kang, C. Freter and W. P. Chen, *Proc. SPIE* **1307**, 276–287 (1990).
5. A. A. Said, M. Sheik-Bahae, D. J. Hagan, T. H. Wei, J. Wang, Y. Young and E. W. Van Stryland, *J. Opt. Soc. Am.* **9**, 405–414 (1992).
6. M. Sheik-Bahae, J. Wang and E. W. Van Stryland, *IEEE J. Quantum Electron.* **30**, 249–255 (1994).
7. T. D. Krauss and F. W. Wise, *Appl. Phys. Lett.* **65**, 1739–1741 (1994).
8. H. Ma, A. S. L. Gomes and G. B. de Araújo, *Opt. Commun.* **87**, 19–22 (1992).
9. M. Bertolottie, G. Liakhou, F. Michelotti, F. Senesi and C. Sibilia, *Pure Appl. Opt.* **1**, 145–156 (1992).
10. V. A. Karavanskii, V. I. Krasovskii, Yu. N. Petrov and A. I. Zavalin, *Laser Phys.* **3**, 1163–1167 (1993).
11. D. C. Rogers, R. J. Manning, B. J. Ainslie, D. Cotter, M. J. Yates, J. M. Parker and S. Morgan, *IEEE Photonics Tech. Lett.* **6**, 1017–1019 (1994).
12. R. Rangel-Rojo, T. Kosa, E. Hajto, P. J. S. Ewen, A. E. Owen, A. K. Kar and B. S. Wherrett, *Opt. Commun.* **109**, 145–150 (1994).
13. T. H. Wei, D. J. Hagan, M. J. Sence, E. W. Van Stryland, J. W. Perry and D. R. Coulter, *Appl. Phys.* **B54**, 46–51 (1992).
14. K. S. Wong and Z. V. Vardeny, *Synthetic Metals* **49**, 13–20 (1992).
15. M. Thakur and R. Quintero-Torres, *Proc. SPIE* **2025**, 446–449 (1993).
16. A. A. Said, C. Wamsley, D. J. Hagan, E. W. Van Stryland, B. A. Reinhardt, P. Roderer and A. G. Dillard, *Chem. Phys. Lett.* **228**, 646–650 (1994).
17. Gang Gu, Wencheng Zhang, Hao Zen, Youwei Du, Yanong Han, Weijun Zhang, Fengzhong Dong and Yuxing Xia, *J. Phys.* **B26**, L451–L455 (1993).
18. D. Paparo, P. Maddalena, G. Abbate, E. Santamato and I. Janossy, *Mol. Cryst. Liq. Cryst.* **251**, 73–84 (1994).
19. L. Li, H. J. Yuan, G. H. Hu and P. Palffy-Muhoray, *Liq. Cryst.* **16**, 703–712 (1994).
20. L. C. Oliveira and S. C. Zilio, *Appl. Phys. Lett.* **65**, 2121–2123 (1994).
21. R. E. Bridges, G. L. Fischer and R. W. Boyd, *Opt. Lett.* **20**, 1821–1823 (1995).
22. T. Xia, D. J. Hagan, M. Sheik-Bahae and E. W. Van Stryland, *Opt. Lett.* **19**, 317–319 (1994).
23. T. Xia, M. Sheik-Bahae, Z. Wang, A. A. Said, D. J. Hagan and E. W. Van Stryland, *Proc. SPIE* **2229**, 148–156 (1994).
24. S. V. Kershaw, *J. Mod. Opt.* **42**, 1361–1366 (1995).
25. M. J. Weber, D. Milam and W. L. Smith, *Opt. Eng.* **17**, 463–469 (1978).
26. J. A. Hermann, *J. Opt. Soc. Am.* **B1**, 729–736 (1984).

27. J. A. Hermann, *Int. J. Nonlin. Opt. Phys.* 1, 541–561 (1992).
28. J. A. Hermann and P. J. Wilson, *Int. J. Nonlin. Opt. Phys.* **2**, 613–629 (1993); Erratum, *Int. J. Nonlin. Opt. Phys.* **3**, 285 (1994).
29. M. Abramowitz and I. A. Stegun (eds), *Handbook of Mathematical Functions*, Dover, New York (1972).
30. J. A. Hermann and P. B. Chapple, *Proc. SPIE* **1307**, 401–413 (1990).
31. J. H. Marburger, *Prog. Quantum Electron.* **4**, 35–110 (1975).
32. M. Sheik-Bahae, A. A. Said, D. J. Hagan, M. J. Soileau and E. W. Van Stryland, *Opt. Eng.* **30**, 1228–1235 (1991).
33. W. Nasalski, *Opt. Commun.* **119**, 218–226 (1995); *J. Opt. Soc. Am.* **B13**, 1736–1747 (1996).
34. C. Paré and P.-A. Bélanger, *Opt. Quantum Electron.* **24**, S1051–S1070 (1992).
35. J. A. Hermann and R. G. McDuff, *J. Opt. Soc. Am.* **B10**, 2056–2064 (1993).
36. P. B. Chapple, J. Staromlynska and R. G. McDuff, *J. Opt. Soc. Am.* **B11**, 975–982 (1994).
37. D. Weaire, B. S. Wherrett, D. A. B. Miller and S. D. Smith, *Opt. Lett.* **4**, 331–333 (1979).
38. R. G. McDuff, "Nonlinear self-focusing and beam propagation using Gaussian Laguerre mode decomposition", Ph. D thesis, Department of Physics, University of Queensland, St Lucia, Qld 4072, Australia (1994).
39. R. G. McDuff, A. E. Smith, N. R. Heckenberg and J. A. Hermann, *Int. J. Nonlin. Opt. Phys.* **1**, 265–286 (1992).
40. S. Hughes, J. M. Burzler, G. Spruce and B. S. Wherrett, *J. Opt. Soc. Am.* **B12**, 1888–1893 (1995).
41. P. B. Chapple and J. A. Hermann, "Power saturation effects in thick, single-element optical limiters", to be published (1997).
42. J. A. Hermann, *Proc. SPIE* **1692**, 56–62 (1992).
43. W. Zhao, J. H. Kim and P. Palffy-Muhoray, *Proc. SPIE* **2229**, 131-147 (1994).
44. S. M. Mian and J. P. Wicksted, *J. Appl. Phys.* **77**, 5434–5436 (1995).
45. S. M. Mian, B. Taheri and J. P. Wicksted, *J. Opt. Soc. Am.* **B13**, 856–863 (1996).
46. A. E. Siegman, *Proc. SPIE* **1224**, 2–14 (1990).
47. P. B. Chapple, *Opt. Eng.* **33**, 2461–2466 (1994).
48. P. B. Chapple and P. J. Wilson, *J. Nonlin. Opt. Phys. and Mtrls* **5**, 419–436 (1996).
49. A. Agnesi, G. C. Reali and A. Tomaselli, *Opt. Lett.* **17**, 1764–1766 (1992).
50. H.-J. Zhang, J.-H. Dai, P.-Y. Wang and L.-A. Wu, *Opt. Lett.* **14**, 695–696 (1989).
51. H. Abdeldayem, W. K. Witherow, A. Shields, B. Penn, D. O. Frazier, M. Moghbel, P. Venkateswarlu, P. Chandra Sekhar and M. C. George, *Opt. Lett.* **19**, 2068–2070 (1994).
52. M. D. Iturbe Castillo, J. J. Sánchez-Mondragón and S. I. Stepanov, *Optik* **100** 49–59 (1995).
53. H. Toda and C. M. Verber, *Opt. Lett.* **17**, 1379–1381 (1992).
54. T.-H. Wei, T.-H. Huang and H.-D. Lin, *Appl. Phys. Lett.* **67**, 2266–2268 (1995).
55. J. Staromlynska, P. B. Chapple, J. R. Davy and T. J. McKay, *Proc. SPIE* **2229**, 59–66 (1994).
56. R. L. Sutherland, *Appl. Opt.* **33**, 5575–5584 (1994).
57. F. Michelotti, F. Caiazza, G. Liakhou, S. Paoloni and M. Bertolotti, *Opt. Commun.* **124**, 103–110 (1996).
58. J.-G. Tian, W.-P. Zang and G. Zhang, *Opt. Commun.* **107**, 415–419 (1994).
59. J.-G. Tian, W.-P. Zang and G. Zhang, *Optik* **98**, 143–146 (1995).
60. A. Marcano O., H. Maillotte, D. Gindre and D. Métin, *Opt. Lett.* **21**, 101–103 (1996).

61. R. DeSalvo, M. Sheik-Bahae, A. A. Said, D. J. Hagan and E. W. Van Stryland, *Opt. Lett.* **18**, 194–196 (1993).
62. T. D. Krauss, J. K. Ranka, F. W. Wise and A. L. Gaeta, *Opt. Lett.* **20**, 1110–1112 (1995).
63. D. V. Petrov, A. S. L. Gomes and Cid B. de Araújo, *Appl. Phys. Lett.* **65**, 1067–1069 (1994).
64. D. V. Petrov, *J. Opt. Soc. Am.* **B13**, 1491–1498 (1996).
65. M. Sheik-Bahae, J. Wang, R. DeSalvo, D. J. Hagan and E. W. Van Stryland, *Opt. Lett.* **17**, 258–260 (1992).
66. H. Ma, A. S. L. Gomes and Cid B. de Araújo, *Appl. Phys. Lett.* **59**, 2666–2668 (1991).
67. J. Wang, M. Sheik-Bahae, A. A. Said, D. J. Hagan and E. W. Van Stryland, *J. Opt. Soc. Am.* **B11**, 1009–1017 (1994).
68. R. W. Boyd, Nonlinear Optics, Academic Press, San Diego, 1992.
69. D. C. Hutchings, M. Sheik-Bahae, D. J. Hagan and E. W. Van Stryland, *Opt. Quantum Electron.* **24**, 1–30 (1992).
70. Y. R. Shen, The Principles of Nonlinear Optics, Wiley, New York, 1984.